Hybrid stochastic kinetic description of two-dimensional traffic dynamics

SIAM J. APPL. MATH.
Vol. 78, No. 5, pp. 2737–2762

HYBRID STOCHASTIC KINETIC DESCRIPTION OF TWO-DIMENSIONAL TRAFFIC DYNAMICS*

MICHAEL HERTY†, ANDREA TOSIN‡, GIUSEPPE VISCONTI†, AND MATTIA ZANELLA‡

Abstract. In this work we present a two-dimensional kinetic traffic model which takes into account speed changes both when vehicles interact along the road lanes and when they change lane. Assuming that lane changes are less frequent than interactions along the same lane and considering that their mathematical description can be done up to some uncertainty in the model parameters, we derive a hybrid stochastic Fokker–Planck–Boltzmann equation in the quasi-invariant interaction limit. By means of suitable numerical methods, precisely structure preserving and direct Monte Carlo schemes, we use this equation to compute theoretical speed-density diagrams of traffic both along and across the lanes, including estimates of the data dispersion, and validate them against real data.

Key words. Boltzmann and Fokker–Planck equations, uncertainty quantification, structure preserving schemes, fundamental diagrams, data dispersion

AMS subject classifications. 35Q20, 35Q70, 35Q84, 90B20

DOI. 10.1137/17M1155909

1. Introduction.

In recent years the legacy of classical kinetic theory has found fruitful applications in the mathematical description of social phenomena [3, 8, 11, 21, 38, 46], including those, such as traffic flow of both vehicles and pedestrians, which mix mechanical and behavioral aspects of the agents [2, 12, 13, 18, 19, 23, 28, 43]. For the sake of completeness, however, we mention that the mathematical modeling of vehicular traffic by means of methods of the kinetic theory has by now a quite long history dating back to the pioneering works [40, 41, 42].

The construction of mathematical models of these phenomena has to face the lack of fundamental principles and background theories: physical forces normally driving the dynamics in classical particle systems like gases and fluids are replaced by empirical interactions among the agents which often are known only statistically; cf., e.g., [5]. Therefore models are in principle characterized by random inputs, such as, e.g., uncertain parameters, which may greatly impact on the realism of the theoretical results with respect to the empirical observations. This is particularly true for models, such as the kinetic ones, which link the individual interactions among the agents to the collective patterns emerging from such interactions. Recent efforts in this direction exploit the uncertainty quantification (UQ) setting; see, e.g., [4, 9, 15, 26, 47] for an introduction. As a matter of fact, UQ methods for stochastic kinetic equations represent a fundamental step toward the actual validation of kinetic models against real data. Some approaches toward the incorporation of data in those models have been also undertaken recently; see, e.g., [17, 22].

*Received by the editors November 7, 2017; accepted for publication (in revised form) August 22, 2018; published electronically October 16, 2018.
http://www.siam.org/journals/siap/78-5/M115590.html
Funding: This work was partially supported by the MIUR-DAAD Joint Mobility Programme and by DFG HE5386/13-15. The fourth author's work was supported by "Compagnia di San Paolo," Turin, Italy.

†Department of Mathematics, IGPM, RWTH Aachen University, Templergraben 55, 52062 Aachen, Germany (herty@igpm.rwth-aachen.de, visconti@igpm.rwth-aachen.de).
‡Department of Mathematical Sciences "G. L. Lagrange," Politecnico di Torino, Corso Duca degli Abruzzi 24, 10129 Turin, Italy (andrea.tosin@polito.it, mattia.zanella@polito.it).

In this paper we propose a new kinetic traffic model, which takes into account speed changes due both to interactions among the vehicles along the road lanes and to lane changes. Although a few traffic models for lane changes are already available in the literature (cf., e.g., [25, 33]), here the novelty consists in the fact that our kinetic model allows us to study the fundamental diagrams of traffic both for the classical case of the flow of vehicles along the lanes and for the flow of vehicles across the lanes, which is instead less classical also from the empirical point of view.

In more detail, besides the acceleration and braking dynamics typical of one-dimensional traffic models along a lane, we suggest that microscopic vehicle dynamics across the lanes are simply a relaxation toward a desired lateral speed, which however is not known deterministically and hence, in our context, plays the role of the aforesaid stochastic parameter. After implementing such microscopic dynamical rules in a stochastic Boltzmann-type equation, owing to the empirical evidence that lane changes are much less frequent than one-to-one vehicle interactions along the lanes, we exploit the quasi-invariant limit technique [46] to finally derive a hybrid Fokker–Planck–Boltzmann equation for the the probability density of the vehicles. In this equation a nonlinear Fokker–Planck operator describes the speed variations along the lanes, whereas a Boltzmann-type collision operator takes into account the speed variations across the lanes. To the best of our knowledge this describes a novel approach to multilane traffic. It is in particular different from kinetic models where lane changing is considered as additional balance terms to a kinetic equation [29]. In fact, the latter modeling does not allow one to account for the intrinsic dynamics across the lanes.

In simplified cases, such as those of mean-field-type interactions among the vehicles, we obtain from the model analytical information on the large-time trend of the system. In particular, we are able to compute the asymptotic probability density of the cars and some of its relevant statistical moments, for instance, the mean and the energy. In the general case, however, the large-time behavior of the model is not known analytically. In order to investigate it accurately, and in particular to find the predicted fundamental diagrams of traffic, we build a suitable numerical scheme for the hybrid stochastic kinetic problem, which in particular extends second order structure preserving (SP) schemes for UQ available in the literature [15, 39] to fully nonlinear Fokker–Planck equations with nonvanishing diffusion. From numerical simulations we observe that the average trend of our model reproduces correctly the fundamental diagrams of traffic both along and across the lanes. Moreover, the quantification of the uncertainty introduced by the stochastic parameter in the dynamics across the lanes proves to be essential in accounting at a theoretical level for the dispersion of the data around the mean normally observed in experimental fundamental diagrams.

Specifically, the rest of the paper is organized as follows. In section 2 we discuss the microscopic models of traffic dynamics along and across the road lanes, which are at the basis of our kinetic model. As usual in kinetic theory, we give them in the form of binary (i.e., one-to-one) interactions among the vehicles. In section 3 we formulate the stochastic Boltzmann-type equation and we study, in a simplified setting, the evolution of some of its thermodynamic-like moments (mean speed and energy), which give insights into the macroscopic trends of the system. In section 4 we derive the hybrid stochastic kinetic model and, again under suitable simplifying assumptions, we investigate its asymptotic distributions. In section 5 we build and test the numerical scheme for the hybrid problem, then we employ it to investigate, also by means of comparison with real data, the fundamental diagrams of traffic produced by the model in the general case. Finally, in section 6 we summarize the main contributions of the work and briefly sketch research perspectives.

TABLE 1
Main variables and parameters of the kinetic model.

Quantity	Description
v_x, v_y	Preinteraction microscopic speeds in the x- and y-direction
w_x, w_y	Microscopic speeds of the leading vehicle in the x- and y-direction
v_x', v_y'	Postinteraction microscopic speeds in the x- and y-direction
W_x, W_y	Reference speeds in the interactions in the x- and y-direction
u_x, u_y	Macroscopic speeds of the flow in the x- and y-direction
V_A, V_B	Target speeds in acceleration and deceleration in the x-direction
Δv	Speed jump in acceleration in the x-direction
$P(\rho)$	Probability of accelerating in the x-direction
v_d	Desired lateral speed (y-direction)

2. Two-dimensional microscopic dynamics. Unlike most kinetic models of vehicular traffic available in the literature, which typically treat the flow of vehicles as one-dimensional, in this paper we consider the case of genuinely two-dimensional velocities describing the flow along the road and across the lanes. In particular, we focus on a space homogeneous approach assuming that the density of the vehicles does not depend on the space position. This setting is very convenient to study the large time behavior of the system. Consistently, the microscopic state of a vehicle will be the pair $\mathbf{v} := (v_x, v_y)$, where v_x is the speed along the road (x-direction) and v_y the lateral speed (y-direction). Notice that v_x can be only positive, because the flow of vehicles in the longitudinal direction of a road is unidirectional, while v_y can be either positive or negative, because lane changes are possible both leftward and rightward. Therefore we assume

$$0 \le v_x \le 1, \qquad |v_y| \le \varepsilon,$$

where $0 < \varepsilon \le 1$ since lateral speeds are in general lower than longitudinal ones. We write

$$\mathbb{V}_x := [0, 1], \qquad \mathbb{V}_y := [-\varepsilon, \varepsilon]$$

for the domains of the two components of the velocity, which have to be understood as dimensionless and referred to suitable characteristic maximal values. The microscopic state space is therefore the set $\mathbb{V} := \mathbb{V}_x \times \mathbb{V}_y \subset \mathbb{R}^2$.

The starting point of a kinetic model is the description of the microscopic speed transitions produced by binary interactions between any two vehicles. In our two-dimensional setting we need to design microscopic interactions both in the x-direction and in the y-direction to account for different dynamics in the two main directions of the flow. In particular, we assume that the interaction frequency *across* the lanes (i.e., in the y-direction) is much smaller than *along* lanes (i.e., in the x-direction) and, consistently, that the x-dynamics modify mainly the speed v_x leaving v_y unaltered, while the y-dynamics modify mainly the speed v_y leaving v_x unaltered. Table 1 summarizes the main variables and parameters which we will use for the description of the microscopic interactions and of the kinetic model.

2.1. Microscopic rules for the x-dynamics. Following [23, 51], we assume that the postinteraction speed v_x' in the x-direction is given by

$$v_x' = \begin{cases} v_x + \alpha P(\rho)(V_A - v_x) + \sqrt{\alpha P(\rho)} D_A(v_x)\xi & \text{if } v_x < W_x, \\ v_x + \alpha(1 - P(\rho))(V_B - v_x) + \sqrt{\alpha(1 - P(\rho))} D_B(v_x)\xi & \text{if } v_x > W_x, \end{cases} \tag{2.1a}$$

where

- $0 < \alpha \leq 1$ is a constant weighting the strength of the interaction;
- $P(\rho) \in [0, 1]$ is the *probability of accelerating* given as a function of the density ρ of the vehicles (cf. [42] and see below for a more detailed discussion);
- V_A, V_B are target speeds in acceleration and deceleration, respectively;
- ξ is a random variable modeling a stochastic fluctuation with zero mean and finite variance $\sigma^2 > 0$, and D_A, $D_B \geq 0$ are diffusion coefficients depending on the speed v_x itself (see below).

From (2.1a) we see that the definition of v_x' depends on the comparison between the current speed v_x and a reference speed $W_x \in [0, 1]$, which discriminates if the vehicle accelerates or brakes. Possible choices for W_x are

$$W_x = w_x \quad \text{or} \quad W_x = u_x,$$

where w_x is the x-component of the velocity $\mathbf{w} := (w_x, w_y)$ of a leading vehicle whereas u_x denotes the mean speed of the flow in x-direction; we refer to [23] for an extensive discussion. If $W_x = w_x$, then we are in the case of genuine *binary* interactions and we assume parallelly that

$$w_x' = w_x, \tag{2.1b}$$

i.e., that the x-speed of the leading vehicle remains unchanged after the interaction. Conversely, if $W_x = u_x$, we are in the case of the so-called *mean-field* interactions, which can be regarded as an approximation of the previous ones; cf. [51].

The probability of accelerating $P = P(\rho)$ is in general a nonincreasing function of the density ρ of the vehicles. In more detail, assuming that $0 \leq \rho \leq 1$, where $\rho = 1$ is the dimensionless value corresponding to the maximum density that can be accommodated in a fully congested road (bumper-to-bumper traffic), one expects that $P \to 1^-$ when $\rho \to 0^+$ and that $P \to 0^+$ when $\rho \to 1^-$. The expression of P that we consider here is in particular

$$P(\rho) := 1 - \rho. \tag{2.2}$$

The target speeds V_A, V_B describe instead the driving style of the individuals. For consistency, we require that $v_x < V_A \leq 1$ and that $0 \leq V_B < v_x$. In [23, 51] several choices of V_A and V_B are discussed along with their influence on the structure of the resulting fundamental diagrams of traffic. In this paper we stick to the modeling of V_A and V_B introduced in [51], namely,

$$V_A := \min\{v_x + \Delta v, 1\}, \qquad V_B := P(\rho) W_x, \tag{2.3}$$

where $\Delta v > 0$ is a fixed parameter denoting the speed jump in acceleration while W_x is the reference speed discussed above.

The local relevance of the stochastic fluctuation ξ, modeling random effects in the choice of the postinteraction speed by the drivers, is weighted by the diffusion coefficients D_A, D_B, which here we consider of the form

$$\begin{aligned} D_A(v_x) &:= \nu(v_x)(V_A - v_x)^\kappa \\ D_B(v_x) &:= \nu(v_x)(v_x - V_B)^\kappa \end{aligned} \qquad \text{with} \quad \nu(v_x) := v_x(1 - v_x) \quad \text{and} \quad \kappa \geq 1; \tag{2.4}$$

cf. [23]. In particular, the function ν makes the stocastic fluctuation vanish at the boundary of $\mathbb{V}_x$ (the x-speed domain), i.e., for $v_x = 0$ and $v_x = 1$.

For a general unbounded stochastic fluctuation $\xi \in \mathbb{R}$ it may happen that the postinteraction speed v_x' resulting from (2.1a) lies outside $\mathbb{V}_x$, implying that not all binary interactions are admissible. In order to prevent this it is sufficient to consider compactly supported stochastic fluctuations as stated in the following result.

PROPOSITION 1. *If*

$$|\xi| \le \min\left\{ \frac{1-\alpha P(\rho)}{\sqrt{\alpha P(\rho)}},\ \frac{1-\alpha(1-P(\rho))}{\sqrt{\alpha(1-P(\rho))}} \right\},$$

then $v_x' \in \mathbb{V}_x$ *for all* $v_x \in \mathbb{V}_x$.

Proof. Let us consider the case $v_x < W_x$ in (2.1a). Since $0 \le V_A - v_x \le 1$, $0 \le \nu(v_x) \le 1$, and $\kappa \ge 1$ we have $D_A(v_x)\xi \le (V_A - v_x)|\xi|$, whence

$$v_x' \le \left(1 - \alpha P(\rho) - \sqrt{\alpha P(\rho)}|\xi|\right) v_x + \left(\alpha P(\rho) + \sqrt{\alpha P(\rho)}|\xi|\right) V_A.$$

If $\alpha P(\rho) + \sqrt{\alpha P(\rho)}|\xi| \le 1$, i.e.,

$$|\xi| \le \frac{1-\alpha P(\rho)}{\sqrt{\alpha P(\rho)}}, \tag{2.5}$$

the right-hand side is a convex combination of v_x, V_A. This implies

$$v_x' \le \max\{v_x, V_A\} = V_A \le 1.$$

On the other hand, since $\nu(v_x) \le v_x$ we also have $D_A(v_x)\xi \ge -v_x|\xi|$ and therefore

$$v_x' \ge \left(1 - \alpha P(\rho) - \sqrt{\alpha P(\rho)}|\xi|\right) v_x + \alpha P(\rho) V_A,$$

which under (2.5) produces $v_x' \ge \alpha P(\rho) V_A \ge 0$. Summarizing, condition (2.5) guarantees that $v_x' \in \mathbb{V}_x$ for all $v_x < W_x$. For the case $v_x > W_x$ in (2.1a) we proceed similarly, thereby deducing also the other bound on $|\xi|$. In fact, we can compute

$$\begin{aligned} v_x' \ge v_x &\left(1 - \alpha(1-P(\rho)) - \sqrt{\alpha(1-P(\rho))}|\xi|\right) \\ &+ V_B \left(\alpha(1-P(\rho)) + \sqrt{\alpha(1-P(\rho))}|\xi|\right). \end{aligned}$$

If $\alpha(1-P(\rho)) + \sqrt{\alpha(1-P(\rho))}|\xi| \le 1$, i.e.,

$$|\xi| \le \frac{1-\alpha(1-P(\rho))}{\sqrt{\alpha(1-P(\rho))}}, \tag{2.6}$$

the right-hand side is a convex combination of v_x, V_B. This implies

$$v_x' \ge \min\{v_x, V_B\} = V_B \ge 0.$$

On the other hand, under (2.6) we also have

$$v_x' \le \left(1 - \left(2\alpha(1-P(\rho)) - 1\right)\right) v_x + V_B \left(2\alpha(1-P(\rho)) - 1\right),$$

and thus $v_x' \le \max\{v_x, V_B\} = v_x \le 1$. In fact, the right-hand side is a convex combination of v_x, V_B since $2\alpha(1-P(\rho)) - 1 \le 1$ holds true. ∎

2.2. Microscopic rules for the *y*-dynamics. We model lane changing as a continuous process in an additional spatial dimension. This dimension is orthogonal to the driving direction and denoted by y. When vehicles move across the lanes (in

y-direction) we consider the following dynamics:

$$v_y' = v_y + \beta(u_x)(v_d(\theta) - v_y). \tag{2.7}$$

Notice that (2.7) accounts neither for binary nor for mean-field interactions. Since lane changes are much less frequent than interactions along the main stream of traffic, the rule (2.7) simply assumes that the lateral speed of the vehicles relaxes toward a *desired speed* $v_d \in \mathbb{V}_y$. However, in order to add realism to the very basic dynamics (2.7), we refrain from fixing deterministically the value of v_d and assume instead that it depends on a random parameter $\theta \in I_\Theta \subseteq \mathbb{R}$. We will come back more precisely to this aspect in the next sections.

The term $\beta(u_x)$ in (2.7) models the relaxation rate toward the stochastic desired speed $v_d(\theta)$. Specifically, it depends on u_x, which is the mean speed in the x-direction, so that the postinteraction speed v_y' across the lanes is affected by the traffic flow along the lanes. Thinking of $v_d(\theta)$ close on average in θ to zero, a conceivable choice is

$$\beta(u_x) \propto u_x,$$

meaning that the faster the flow along the lanes the faster the relaxation toward $v_d(\theta)$, namely, toward zero on average in θ, across the lanes, consistently with the intuition that lane changes are not necessary if the traffic is sufficiently fluent in the driving directions.

Similarly to the x-dynamics discussed in section 2.1, also for (2.7) we need to ensure that $v_y' \in \mathbb{V}_y$ for all $v_y \in \mathbb{V}_y$. The following result holds.

PROPOSITION 2. *If $\beta : [0, 1] \to [0, 1]$, then $v_y' \in \mathbb{V}_y$ for all $v_y \in \mathbb{V}_y$.*

Proof. By rewriting (2.7) as $v_y' = (1 - \beta(u_x))v_y + \beta(u_x)v_d(\theta)$ we see that, under the assumption $0 \le \beta(u_x) \le 1$, the postinteraction speed v_y' is a convex combination of v_y, $v_d(\theta) \in \mathbb{V}_y$. Hence the thesis easily follows from the convexity of $\mathbb{V}_y$. ∎

3. Stochastic Boltzmann-type description. The interaction rules (2.1a)–(2.1b), (2.7) can be encoded in a kinetic Boltzmann-type description of the dynamics. This is particularly useful to study the asymptotic macroscopic trends of the system, possibly taking advantage of suitable scaling and limit procedures.

For a certain realization $\theta \in I_\Theta$ of the random parameter appearing in (2.7), let

$$f = f(\mathbf{v}, t; \theta) : \mathbb{V} \times [0, +\infty) \to \mathbb{R}_+$$

be the probability distribution function such that $f(\mathbf{v}, t; \theta)\, d\mathbf{v}$ is the fraction of vehicles which at time $t \ge 0$ have a microscopic speed in an infinitesimal volume of the state space $\mathbb{V}$ centered at $\mathbf{v}$. Since θ is a constant parameter in each y-interaction, whose precise value is however unknown, we proceed along the lines of the so-called UQ: we first consider the family of all possible dynamics of the system for $\theta \in I_\Theta$, which amounts to regarding f as parametrized by θ; next we average their outputs according to the probability distribution of θ, say, $h = h(\theta) : I_\Theta \to \mathbb{R}_+$ such that $\int_{I_\Theta} h(\theta)\, d\theta = 1$. We refer to [47] for more details.

According to standard arguments in kinetic theory (see, e.g., [36] and references therein), the time evolution of f is given by the following dimensionless Boltzmann-

type kinetic equation in weak form:

(3.1)
$$\frac{d}{dt}\int_{\mathbb{V}}\varphi(\mathbf{v})f(\mathbf{v},\,t;\,\theta)\,d\mathbf{v} = \frac{\rho}{2}\left\langle\int_{\mathbb{V}}\int_{\mathbb{V}}\left(\varphi(\mathbf{v}'_x)-\varphi(\mathbf{v})\right)f(\mathbf{v},\,t;\,\theta)f(\mathbf{w},\,t;\,\theta)\,d\mathbf{v}\,d\mathbf{w}\right\rangle + \gamma\rho\int_{\mathbb{V}}\left(\varphi(\mathbf{v}'_y)-\varphi(\mathbf{v})\right)f(\mathbf{v},\,t;\,\theta)\,d\mathbf{v},$$

where the following hold:

- $\varphi:\mathbb{V}\to\mathbb{R}$ is a test function, i.e., any function depending on the microscopic state $\mathbf{v}$.
- The first term at the right-hand side accounts for the interactions in the x-direction which leave the speed v_y unaltered; in particular, $\mathbf{v}'_x := (v'_x,\,v_y)$ with v'_x given by (2.1a). The coefficient $\rho/2$ is the interaction rate, which is supposed to be proportional to the density of the vehicles and, in particular, takes into account the asymmetric form of the interactions (2.1a)–(2.1b) (cf. [48]).
- $\langle\cdot\rangle$ denotes the expectation with respect to the stochastic fluctuation ξ (cf. (2.1a)).
- The second term at the right-hand side accounts for speed changes in the y-direction which leave the speed v_x unaltered; in particular, $\mathbf{v}'_y := (v_x,\,v'_y)$ with v'_y given by (2.7). The coefficient $\gamma\rho$ is the interaction rate, with $0<\gamma\ll 1$ modeling the much lower frequency of the interactions across the lanes with respect to those along the lanes.

It is worth pointing out that (3.1) is a *stochastic* Boltzmann-type equation, because it is parametrized by the random parameter θ. From the knowledge of the kinetic distribution function f one can compute θ-expected quantities, such as the expected distribution function and its θ-variance:

(3.2)
$$\bar{f}(\mathbf{v},\,t) := \int_{I_\Theta} f(\mathbf{v},\,t;\,\theta)h(\theta)\,d\theta, \qquad \mathrm{Var}_\theta(f)(\mathbf{v},\,t) := \int_{I_\Theta} f^2(\mathbf{v},\,t;\,\theta)h(\theta)\,d\theta - \bar{f}^2(\mathbf{v},\,t).$$

Similarly, from the thermodynamic-like moments of f parametrized by θ,

$$M_\varphi(t;\,\theta) := \int_{\mathbb{V}}\varphi(\mathbf{v})f(\mathbf{v},\,t;\,\theta)\,d\mathbf{v},$$

one can recover the average expected $\mathbf{v}$-moments and their θ-variance:

$$\bar{M}_\varphi(t) := \int_{I_\Theta} M_\varphi(t;\,\theta)h(\theta)\,d\theta = \int_{\mathbb{V}}\varphi(\mathbf{v})\bar{f}(\mathbf{v},\,t)\,d\mathbf{v},$$
$$\mathrm{Var}_\theta(M_\varphi)(t) := \int_{I_\Theta} M^2(t;\,\theta)h(\theta)\,d\theta - \bar{M}^2_\varphi(t),$$

which are useful tools for quantifying the uncertainty induced in the system dynamics by the random parameter θ. Notice that from (3.1) it is in general not possible to derive a closed equation for $\bar{f}(\mathbf{v},\,t)$ by simply integrating both sides with respect to $h(\theta)\,d\theta$.

3.1. Evolution of the macroscopic quantities. First, from (3.1) with $\varphi(\mathbf{v}) = 1$ we obtain that the integral of f with respect to $\mathbf{v}$ is conserved in time for all $\theta\in I_\Theta$. Hence, if $f(\cdot,\,t;\,\theta)$ is chosen to be a probability density at $t=0$ it will be so for all

$t > 0$. The physical counterpart of this fact is the conservation of the mass of vehicles, whose density is fixed by the parameter $\rho \in [0, 1]$ appearing in (2.1a) and (3.1).

Let us now consider any pth order moment, $p \in \mathbb{N}$, of f in the x-direction, which amounts to taking $\varphi(\mathbf{v}) = v_x^p$. Plugging into (3.1) we get

$$\frac{d}{dt}\int_{\mathbb{V}} v_x^p f(\mathbf{v}, t; \theta)\, d\mathbf{v} = \frac{\rho}{2}\left\langle \int_{\mathbb{V}}\int_{\mathbb{V}} ((v_x')^p - v_x^p)\, f(\mathbf{v}, t; \theta) f(\mathbf{w}, t; \theta)\, d\mathbf{v}\, d\mathbf{w} \right\rangle, \tag{3.3}$$

because $\varphi(\mathbf{v}_y') - \varphi(\mathbf{v}) = v_x^p - v_x^p = 0$. Similarly, if we consider any pth order moment of f in the y-direction, i.e., if we take $\varphi(\mathbf{v}) = v_y^p$, we discover

$$\frac{d}{dt}\int_{\mathbb{V}} v_y^p f(\mathbf{v}, t; \theta)\, d\mathbf{v} = \gamma\rho \int_{\mathbb{V}} \left((v_y')^p - v_y^p\right) f(\mathbf{v}, t; \theta)\, d\mathbf{v}, \tag{3.4}$$

because now $\varphi(\mathbf{v}_x') - \varphi(\mathbf{v}) = v_y^p - v_y^p = 0$.

This argument implies that the evolution of the macroscopic quantities in the single directions of the traffic flow may be obtained from (3.1) by considering separately the two collision operators at the right-hand side. Notice, however, that it is in general not possible to reconstruct the kinetic distribution function $f(\cdot, t; \theta)$ on the whole space $\mathbb{V}$ of the microscopic states by taking in (3.1) test functions which depend on only one of the two speeds, namely, by looking at the dynamics in only one direction.

3.1.1. Macroscopic x-dynamics: The synchronized flow case. We now investigate in more detail the evolution equations of some macroscopic quantities in the x-direction. Precisely, we consider (2.1a)–(2.1b) and (3.3) in the simplified setting

$$V_A = u_x, \quad V_B = u_x, \quad W_x = u_x,$$

which makes possible some explicit analytical computations.

The time evolution of the x-mean speed $u_x = u_x(t; \theta)$ results from (3.3) with $p = 1$. In particular, recalling that the stochastic fluctuation ξ is a centered random variable, we obtain

$$\begin{aligned}\frac{du_x}{dt} = \frac{\alpha\rho}{2}\Bigg(&P(\rho)\int_{-\varepsilon}^{\varepsilon}\int_0^{u_x}(u_x - v_x) f(\mathbf{v}, t; \theta)\, dv_x\, dv_y \\ &+ (1 - P(\rho))\int_{-\varepsilon}^{\varepsilon}\int_{u_x}^{1}(u_x - v_x) f(\mathbf{v}, t; \theta)\, dv_x\, dv_y\Bigg).\end{aligned}$$

Now, observing that

$$\begin{aligned}&\int_{-\varepsilon}^{\varepsilon}\int_0^{u_x}(u_x - v_x) f(\mathbf{v}, t; \theta)\, dv_x\, dv_y + \int_{-\varepsilon}^{\varepsilon}\int_{u_x}^{1}(u_x - v_x) f(\mathbf{v}, t; \theta)\, dv_x\, dv_y \\ &\quad = \int_{\mathbb{V}}(u_x - v_x) f(\mathbf{v}, t; \theta)\, d\mathbf{v} = 0,\end{aligned}$$

we get

$$\frac{du_x}{dt} = \begin{cases} \dfrac{\alpha\rho}{2}(2P(\rho) - 1)\displaystyle\int_{-\varepsilon}^{\varepsilon}\int_0^{u_x}(u_x - v_x) f(\mathbf{v}, t; \theta)\, dv_x\, dv_y, \\ \dfrac{\alpha\rho}{2}(1 - 2P(\rho))\displaystyle\int_{-\varepsilon}^{\varepsilon}\int_{u_x}^{1}(u_x - v_x) f(\mathbf{v}, t; \theta)\, dv_x\, dv_y, \end{cases}$$

whence finally, summing the two equations,

$$\frac{du_x}{dt} = \frac{\alpha\rho}{4}(2P(\rho)-1)\int_{\mathbb{V}} |u_x - v_x| f(\mathbf{v},\, t;\, \theta)\, d\mathbf{v}.$$

By defining the marginal distribution $f_x(v_x,\, t;\, \theta) := \int_{-\varepsilon}^{\varepsilon} f(\mathbf{v},\, t;\, \theta)\, dv_y$, we notice that at the right-hand side it results in $\int_{\mathbb{V}} |u_x - v_x| f(\mathbf{v},\, t;\, \theta)\, d\mathbf{v} = 0$ if and only if $f_x(v_x,\, t;\, \theta) = \delta_{u_x}(v_x)$. Therefore, if $\rho(2P(\rho)-1) \neq 0$, the only steady state in the x-direction, which allows for a stationary mean speed, is the *synchronized traffic* with all the vehicles travelling at the same speed [27]. Conversely, for $f_x(v_x,\, t;\, \theta) \neq \delta_{u_x}(v_x)$ (and $\rho \neq 0$) the mean speed either increases or decreases in time depending on the sign of $2P(\rho)-1$. In particular, it increases for $P(\rho) > \frac{1}{2}$, which defines the so-called *free phase* of traffic when the vehicle density is small (recall that the mapping $\rho \mapsto P(\rho)$ is nonincreasing), whereas it decreases for $P(\rho) < \frac{1}{2}$, which defines the so-called *congested phase* of traffic when the vehicle density is large. The value $\rho = \rho_c$ such that $P(\rho_c) = \frac{1}{2}$ is called the *critical density*. For the function (2.2) it results, for instance, in $\rho_c = \frac{1}{2}$, which is consistent with the values found in [43, 44, 45] for different kinetic models of traffic flow.

In order to further explore the macroscopic trends of the model it is useful to investigate also the evolution of the energy along the lanes, say, $E_x = E_x(t;\, \theta)$, namely the second order x-moment of f obtained by taking $p = 2$ in (3.3). Since the complete equation for E_x is quite complicated, we conveniently resort to a particular limit procedure, called the *quasi-invariant interaction limit* [46], which allows us to grasp the essential time-asymptotic behavior of E_x. This technique is inspired by the so-called *grazing collision limit* introduced in the classical kinetic theory in [49]; see also [20, 36]. Specifically, in (2.1a) we consider the regime of weak but frequent interactions. This corresponds to taking α small (notice that α tunes both the strength of the speed variation and the variance of the stochastic fluctuation) and to simultaneously scaling the time as $\tau := \alpha t$. In practice, we pass from the characteristic t-scale of single microscopic interactions to a larger time scale defined by the variable τ. Introducing the scaled kinetic distribution function $g(\mathbf{v},\, \tau;\, \theta) := f(\mathbf{v},\, \tau/\alpha;\, \theta)$ and noticing that $\partial_\tau g = \frac{1}{\alpha}\partial_t f$ we obtain from (3.3) with $p = 2$ the equation

$$\frac{dE_x}{d\tau} = \frac{\rho}{2\alpha}\left\langle \int_{\mathbb{V}}\int_{\mathbb{V}} \left((v_x')^2 - v_x^2\right) g(\mathbf{v},\, \tau;\, \theta) g(\mathbf{w},\, \tau;\, \theta)\, d\mathbf{v}\, d\mathbf{w} \right\rangle,$$

whence, using (2.1a) together with $\langle \xi \rangle = 0$, $\langle \xi^2 \rangle = \sigma^2$ and letting $\alpha \to 0^+$,

$$\begin{aligned} &= \frac{\sigma^2\rho}{2}\left(P(\rho)\int_{-\varepsilon}^{\varepsilon}\int_0^{u_x} D_A^2(v_x) g(\mathbf{v},\, \tau;\, \theta)\, dv_x\, dv_y \right. \\ &\qquad \left. + (1-P(\rho))\int_{-\varepsilon}^{\varepsilon}\int_{u_x}^{1} D_B^2(v_x) g(\mathbf{v},\, \tau;\, \theta)\, dv_x\, dv_y \right) \\ &\quad + \frac{\rho}{2}\left(u_x^2 - E_x\right) - \frac{\rho}{2}(1-2P(\rho))\int_{\mathbb{V}} v_x |u_x - v_x| g(\mathbf{v},\, \tau;\, \theta)\, d\mathbf{v}. \end{aligned}$$

In particular, in the absence of stochastic fluctuation ($\sigma^2 = 0$) this equation specializes as

$$\frac{dE_x}{d\tau} = \frac{\rho}{2}\left(u_x^2 - E_x\right) - \frac{\rho}{2}(1-2P(\rho))\int_{\mathbb{V}} v_x |u_x - v_x| g(\mathbf{v},\, \tau;\, \theta)\, d\mathbf{v}.$$

The term $u_x^2 - E_x$ at the right-hand side is the opposite of the variance of the microscopic speeds in the x-direction, and therefore it is nonpositive. Moreover, for $P(\rho) \leq \frac{1}{2}$, namely, in the congested phase of traffic, also the second term at the right-hand side is nonpositive, which makes the energy on the whole nonincreasing in time. Conversely, for $P(\rho) > \frac{1}{2}$, namely, in the free phase of traffic, the second term at the right-hand side is nonnegative, and thus in principle the energy may not be monotonic in this case. This implies that the convergence to the steady state $E_x \to u_x^2$, consistent with the asymptotic state of synchronized traffic discussed before, is in general smoother in the congested than in the free phase of traffic.

Finally, we stress that also in the case $\sigma^2 > 0$ the full equation of E_x gives an asymptotic trend of the energy consistent with the synchronized traffic (i.e., $E_x \to u_x^2$) thanks to the fact that with the definition (2.4) it results in $D_A(u_x) = D_B(u_x) = 0$.

3.1.2. Macroscopic *y*-dynamics. We now study the evolution of the mean speed $u_y = u_y(t;\theta)$ and energy $E_y = E_y(t;\theta)$ of traffic in the y-direction taking advantage of (3.4) complemented with the microscopic dynamics (2.7).

For $p = 1$ we get

$$\frac{du_y}{dt} = \gamma\rho\beta(u_x)(v_d(\theta) - u_y),$$

and therefore asymptotically ($\frac{du_y}{dt} \to 0$) it results in $u_y \to v_d(\theta)$, consistently with microscopic relaxation dynamics toward the desired speed v_d.

To investigate the asymptotic trend of the energy E_y it is convenient to resort also in this case to the quasi-invariant interaction limit. For this, we assume, for instance, $\beta(u_x) = \beta_0 u_x$, $0 < \beta_0 \leq 1$, and we consider the regime of small β_0. By scaling the time as $\tau := \beta_0 t$ and the distribution function as $g(\mathbf{v}, \tau; \theta) := f(\mathbf{v}, \tau/\beta_0; \theta)$ we obtain from (3.4)

$$\frac{d}{d\tau}\int_{\mathbb{V}} v_y^p g(\mathbf{v}, \tau; \theta)\, d\mathbf{v} = \frac{\gamma\rho}{\beta_0}\int_{\mathbb{V}} \left((v_y')^p - v_y^p\right) g(\mathbf{v}, \tau; \theta)\, d\mathbf{v},$$

whence, for $p = 2$ and using (2.7) in the limit $\beta_0 \to 0^+$,

$$\frac{dE_y}{d\tau} = 2\gamma\rho u_x(v_d(\theta)u_y - E_y),$$

which asymptotically ($\frac{dE_y}{d\tau} \to 0$) produces $E_y \to v_d(\theta)u_y \to v_d^2(\theta)$. This implies that the speed variance in the y-direction tends to zero, namely, that $f_y(v_y, t; \theta) \to \delta_{v_d(\theta)}(v_y)$, where f_y denotes the marginal distribution $f_y(v_y, t; \theta) := \int_0^1 f(\mathbf{v}, t; \theta)\, dv_x$.

4. Hybrid kinetic model. Considering again the full Boltzmann-type equation (3.1) with general terms V_A, V_B, W_x in (2.1a), we now use the quasi-invariant interaction limit introduced in section 3.1.1 to derive a hybrid kinetic model under the assumption of different interaction frequency among the vehicles along and across the lanes; cf. section 2. The advantage of the resulting model is that it is simpler than (3.1) but it still preserves the main features of the asymptotic dynamics of the Boltzmann-type model. In more detail, the nonlinear integral collision operator in the x-direction (the first term at the right-hand side of (3.1)) is replaced by a *Fokker–Planck-type transport-diffusion differential operator* which describes the *mean-field* effect of the frequent interactions among the vehicles along the lanes. Parallelly, the linear collision operator in the y-direction (the second term at the right-hand side of (3.1)) remains to describe the rare interactions among the vehicles across the road lanes.

As already mentioned, the quasi-invariant interaction limit has been introduced in [46] (see also [36]) as an asymptotic procedure reminiscent of the *grazing collision limit* in classical kinetic theory [14, 16, 37, 50]. Since then it has been widely used in the literature to study the large-time trends of, e.g., traffic flow models [23, 51], crowd dynamics models [19], opinion formation models [3], and socio-economic models [11, 21].

4.1. The Fokker–Planck–Boltzmann model. The regime that we want to study is characterized by a small value of the parameter α in (2.1a), corresponding to weak interactions in the x-direction, and by a simultaneously small value of the parameter γ in (3.1), corresponding to rare interactions in the y-direction with respect to those in the x-direction. As before, we introduce the time scale $\tau := \alpha t$, where the frequency of the x-binary interactions raises to $O(1/\alpha)$, and we scale the distribution function as $g(\mathbf{v}, \tau; \theta) := f(\mathbf{v}, \tau/\alpha; \theta)$. Notice that for α small we have $t = \tau/\alpha$ large, and hence the limit $\alpha \to 0^+$ describes the asymptotic trend of f. On the other hand, in view of the previous definition, the asymptotic trend of f is well approximated by that of g.

Since $\partial_\tau g = \frac{1}{\alpha}\partial_t f$, from (3.1) we get

$$\frac{d}{d\tau}\int_{\mathbb{V}} \varphi(\mathbf{v}) g(\mathbf{v}, \tau; \theta)\, d\mathbf{v} = \frac{\rho}{2\alpha}\left\langle \int_{\mathbb{V}}\int_{\mathbb{V}} \left(\varphi(\mathbf{v}'_x) - \varphi(\mathbf{v})\right) g(\mathbf{v}, \tau; \theta) g(\mathbf{w}, \tau; \theta)\, d\mathbf{v}\, d\mathbf{w}\right\rangle + \frac{\gamma}{\alpha}\rho \int_{\mathbb{V}} \left(\varphi(\mathbf{v}'_y) - \varphi(\mathbf{v})\right) g(\mathbf{v}, \tau; \theta)\, d\mathbf{v}. \tag{4.1}$$

Let us pick a smooth test function with compact support $\varphi \in C^3_c(\mathbb{V})$. Expanding the difference $\varphi(\mathbf{v}'_x) - \varphi(\mathbf{v})$ at the right-hand side we have

$$\varphi(\mathbf{v}'_x) - \varphi(\mathbf{v}) = \partial_{v_x}\varphi(\mathbf{v})(v'_x - v_x) + \frac{1}{2}\partial^2_{v_x}\varphi(\mathbf{v})(v'_x - v_x)^2 + \frac{1}{6}\partial^3_{v_x}\varphi(\bar{\mathbf{v}}_x)(v'_x - v_x)^3,$$

where $\bar{\mathbf{v}}_x := (\bar{v}_x, v_y)$ is a point such that $\min\{v_x, v'_x\} < \bar{v}_x < \max\{v_x, v'_x\}$. Using the expression of v'_x given in (2.1a) with $\langle \xi \rangle = 0$, $\langle \xi^2 \rangle = \sigma^2$ and plugging this expansion into (4.1) we discover

$$\begin{aligned}
&\frac{d}{d\tau}\int_{\mathbb{V}} \varphi(\mathbf{v}) g(\mathbf{v}, \tau; \theta)\, d\mathbf{v} \\
&\quad = -\frac{\rho}{2}\int_{\mathbb{V}}\int_{\mathbb{V}} \partial_{v_x}\varphi(\mathbf{v}) L(v_x, V_A, V_B, W_x) g(\mathbf{v}, \tau; \theta) g(\mathbf{w}, \tau; \theta)\, d\mathbf{v}\, d\mathbf{w} \\
&\qquad + \frac{\sigma^2\rho}{4}\int_{\mathbb{V}}\int_{\mathbb{V}} \partial^2_{v_x}\varphi(\mathbf{v}) D^2(v_x, W_x) g(\mathbf{v}, \tau; \theta) g(\mathbf{w}, \tau; \theta)\, d\mathbf{v}\, d\mathbf{w} \\
&\qquad + R_\alpha(\varphi) \\
&\qquad + \frac{\gamma}{\alpha}\rho \int_{\mathbb{V}} \left(\varphi(\mathbf{v}'_y) - \varphi(\mathbf{v})\right) g(\mathbf{v}, \tau; \theta)\, d\mathbf{v},
\end{aligned} \tag{4.2}$$

where we have denoted for brevity

$$L(v_x, V_A, V_B, W_x) := \begin{cases} P(\rho)(v_x - V_A) & \text{if } v_x < W_x, \\ (1 - P(\rho))(v_x - V_B) & \text{if } v_x > W_x, \end{cases}$$
$$D(v_x, W_x) := \begin{cases} \sqrt{P(\rho)} D_A(v_x) & \text{if } v_x < W_x, \\ \sqrt{1 - P(\rho)} D_B(v_x) & \text{if } v_x > W_x. \end{cases} \tag{4.3}$$

Furthermore the term $R_\alpha(\varphi)$ is

$$\begin{aligned}
&R_\alpha(\varphi)\\
&\quad := -\frac{\alpha\rho}{4}\int_{\mathbb{V}}\int_{\mathbb{V}}\partial^2_{v_x}\varphi(\mathbf{v})L(v_x, V_A, V_B, W_x)g(\mathbf{v}, \tau; \theta)g(\mathbf{w}, \tau; \theta)\,d\mathbf{v}\,d\mathbf{w}\\
&\qquad -\frac{\alpha^2\rho}{12}\int_{\mathbb{V}}\int_{\mathbb{V}}\partial^3_{v_x}\varphi(\bar{\mathbf{v}}_x)L^3(v_x, V_A, V_B, W_x)g(\mathbf{v}, \tau; \theta)g(\mathbf{w}, \tau; \theta)\,d\mathbf{v}\,d\mathbf{w}\\
&\qquad -\frac{\alpha\sigma^2\rho}{4}\int_{\mathbb{V}}\int_{\mathbb{V}}\partial^3_{v_x}\varphi(\bar{\mathbf{v}}_x)L(v_x, V_A, V_B, W_x)D^2(v_x, W_x)g(\mathbf{v}, \tau; \theta)g(\mathbf{w}, \tau; \theta)\,d\mathbf{v}\,d\mathbf{w}\\
&\qquad +\frac{\sqrt{\alpha}\rho}{12}\langle\xi^3\rangle\int_{\mathbb{V}}\int_{\mathbb{V}}\partial^3_{v_x}\varphi(\bar{\mathbf{v}}_x)D^3(v_x, W_x)g(\mathbf{v}, \tau; \theta)g(\mathbf{w}, \tau; \theta)\,d\mathbf{v}\,d\mathbf{w}
\end{aligned}$$

and is such that

$$\begin{aligned}
|R_\alpha(\varphi)| \le{}& \frac{\alpha\rho}{4}\left\|\partial^2_{v_x}\varphi\right\|_\infty\|L\|_\infty + \frac{\alpha^2\rho}{12}\left\|\partial^3_{v_x}\varphi\right\|_\infty\|L\|^3_\infty\\
&+\frac{\alpha\sigma^2\rho}{4}\left\|\partial^3_{v_x}\varphi\right\|_\infty\|L\|_\infty\|D\|^2_\infty + \frac{\sqrt{\alpha}\rho}{12}\langle|\xi|^3\rangle\left\|\partial^3_{v_x}\varphi\right\|_\infty\|D\|^3_\infty,
\end{aligned}$$

where $\|\cdot\|_\infty$ is the ∞-norm in $\mathbb{V}$. Since L and D are bounded and ξ has finite moments of any order thanks to Proposition 1, we deduce $R_\alpha(\varphi)\to 0$ for $\alpha\to 0^+$.

Finally, taking the limit $\alpha\to 0^+$, $\gamma\to 0^+$ in (4.2) and assuming $\gamma/\alpha = O(1)$, i.e., $\gamma/\alpha\to\mu>0$, we obtain

$$\begin{aligned}
\frac{d}{d\tau}\int_{\mathbb{V}}\varphi(\mathbf{v})g(\mathbf{v}, \tau; \theta)\,d\mathbf{v} = &-\int_{\mathbb{V}}\partial_{v_x}\varphi(\mathbf{v})\mathcal{L}[g](v_x, \tau; \theta)g(\mathbf{v}, \tau; \theta)d\mathbf{v}\\
&+\frac{\sigma^2}{2}\int_{\mathbb{V}}\partial^2_{v_x}\varphi(\mathbf{v})\mathcal{D}[g](v_x, \tau; \theta)g(\mathbf{v}, \tau; \theta)\,d\mathbf{v}\\
&+\mu\rho\int_{\mathbb{V}}\left(\varphi(\mathbf{v}'_y)-\varphi(\mathbf{v})\right)g(\mathbf{v}, \tau; \theta)\,d\mathbf{v},
\end{aligned}\tag{4.4}$$

where we have denoted

$$\begin{aligned}
\mathcal{L}[g](v_x, \tau; \theta) &:= \frac{\rho}{2}\int_{\mathbb{V}}L(v_x, V_A, V_B, W_x)g(\mathbf{w}, \tau; \theta)\,d\mathbf{w},\\
\mathcal{D}[g](v_x, \tau; \theta) &:= \frac{\rho}{2}\int_{\mathbb{V}}D^2(v_x, W_x)g(\mathbf{w}, \tau; \theta)\,d\mathbf{w}.
\end{aligned}\tag{4.5}$$

Integrating back by parts the right-hand side of (4.4) and recalling the compactness of the support of φ we see that, owing to the arbitrariness of φ, (4.4) is a weak form of the equation

$$\partial_\tau g = \partial_{v_x}\left(\mathcal{L}[g]g + \frac{\sigma^2}{2}\partial_{v_x}(\mathcal{D}[g]g)\right) + \mu\rho Q_y(g),\tag{4.6}$$

where

$$Q_y(g) = Q_y(g)(\mathbf{v}, \tau; \theta) = \frac{1}{1-\beta(u_x)}g({}'\mathbf{v}_y, \tau; \theta) - g(\mathbf{v}, \tau; \theta)$$

is the strong form of the Boltzmann-type collision operator in the y-direction. Specifically, ${}'\mathbf{v}_y := (v_x, {}'v_y)$ denotes the preinteraction velocity yielding $\mathbf{v} = (v_x, v_y)$ as

postinteraction velocity according to (2.7), i.e., $'v_y = \frac{v_y - \beta(u_x)v_d(\theta)}{1-\beta(u_x)}$, while the coefficient $\frac{1}{1-\beta(u_x)}$ is the Jacobian of the transformation (2.7).

Equation (4.6) represents our *hybrid kinetic model*, featuring at the right-hand side the Fokker–Planck-type operator

$$\partial_{v_x}\left(\mathcal{L}[g]g + \frac{\sigma^2}{2}\partial_{v_x}(\mathcal{D}[g]g)\right)$$

for the frequent vehicle interactions in the x-direction complemented with the linear collision operator $Q_y(g)$ for the less frequent speed changes in the y-direction. The constant $\mu > 0$ permits to tune the relative importance of the two terms.

Remark 1. Equation (4.4), hence (4.6), has been obtained from (4.2) assuming that $\gamma/\alpha = O(1)$ for $\alpha, \gamma \to 0^+$. Other asymptotic regimes may be considered as well, among which we mention in particular the one with $\gamma/\alpha = o(1)$. It corresponds to interactions across the lanes so rare that for large times one recovers a classical one-dimensional traffic model with only x-dynamics along the lanes (in practice, (4.6) without the collision term $Q_y(g)$). Clearly, the choice leading to (4.6) is the one which guarantees a correct balance between the two contributions, thereby allowing one to study genuinely two-dimensional traffic dynamics with the proper frequencies.

4.2. Asymptotic distributions. As stated at the beginning of section 4, model (4.6) preserves the macroscopic trends of the original Boltzmann-type model (3.1). In particular, the large-time behavior of g is the same as that of f under the quasi-invariant interaction limit; cf. section 4.1. Owing to the results of section 3.1.2, this allows us to conclude immediately that $g_y(v_y, \tau; \theta) \to \delta_{v_d(\theta)}(v_y)$ for $\tau \to +\infty$, where $g_y(v_y, \tau; \theta) := \int_0^1 g(\mathbf{v}, \tau; \theta)\, dv_x$.

More in general, assuming for simplicity that $\beta(u_x) \equiv \beta_0 > 0$ in (2.7), so that the microscopic x- and y-dynamics are decoupled, we can look for asymptotic distributions $g^\infty = g^\infty(\mathbf{v}; \theta)$ of the form

$$g^\infty(\mathbf{v}; \theta) = g_x^\infty(v_x) g_y^\infty(v_y; \theta).$$

Plugging this representation into (4.6) yields

$$g_y^\infty \partial_{v_x}\left(\mathcal{L}[g_x^\infty]g_x^\infty + \frac{\sigma^2}{2}\partial_{v_x}(\mathcal{D}[g_x^\infty]g_x^\infty)\right) + \mu\rho g_x^\infty Q_y(g_y^\infty) = 0, \tag{4.7}$$

where

$$\mathcal{L}[g_x^\infty](v_x) = \frac{\rho}{2}\int_0^1 L(v_x, V_A, V_B, W_x) g_x^\infty(w_x)\, dw_x$$

$$\mathcal{D}[g_x^\infty](v_x) = \frac{\rho}{2}\int_0^1 D^2(v_x, W_x) g_x^\infty(w_x)\, dw_x$$

$$Q_y(g_y^\infty)(v_y; \theta) = \frac{1}{1-\beta_0} g_y^\infty('v_y; \theta) - g_y^\infty(v_y; \theta).$$

Besides the already determined $g_y^\infty(v_y; \theta) = \delta_{v_d(\theta)}(v_y)$, which is such that $Q_y(g_y^\infty) = 0$ (in the proper weak sense; cf. (4.4)), from (4.7) we see that the asymptotic marginal distribution g_x^∞ in the x-direction is determined by setting

$$\mathcal{L}[g_x^\infty]g_x^\infty + \frac{\sigma^2}{2}\partial_{v_x}(\mathcal{D}[g_x^\infty]g_x^\infty) = 0.$$

The way in which this equation can be solved may be strictly dependent on the choice of the terms V_A, V_B, W_x in (2.1a). For instance, from section 3.1.1 we know that for

$V_A = V_B = W_x = u_x$ we should expect $g_x^\infty(v_x;\,\theta) = \delta_{u_x}(v_x)$ (again in the proper weak sense; cf. (4.4)). In a more general case, when we only assume $W_x = u_x$ and admit that V_A, V_B may be functions of v_x, i.e., $V_A = V_A(v_x)$ and $V_B = V_B(v_x)$, following [51] we determine

$$g_x^\infty(v_x) = \begin{cases} C_A \left(\dfrac{V_A(u_x) - u_x}{V_A(v_x) - v_x} \right)^2 \exp\left(-\dfrac{2}{\sigma^2} \displaystyle\int_{v_x}^{u_x} \frac{1}{V_A(v) - v}\, dv \right) & \text{if } v_x < u_x, \\ C_B \left(\dfrac{u_x - V_B(u_x)}{v_x - V_B(v_x)} \right)^2 \exp\left(-\dfrac{2}{\sigma^2} \displaystyle\int_{u_x}^{v_x} \frac{1}{v - V_B(v)}\, dv \right) & \text{if } v_x > u_x, \end{cases} \tag{4.8}$$

where $C_A, C_B > 0$ are normalization constants to be fixed in such a way that $\int_0^1 g_x^\infty(v_x)\, dv_x = 1$ and $\int_0^1 v_x g_x^\infty(v_x)\, dv_x = u_x$.

Remark 2. We refer to the already mentioned paper [51] for detailed expressions of g_x^∞ in case of several choices of V_A, V_B including (2.3). We simply remark that for $V_A = V_B = u_x$ (4.8) gives $g_x^\infty(v_x) = 0$ for $v_x \neq u_x$, which is indeed consistent with the true distributional solution $g_x^\infty(v_x) = \delta_{u_x}(v_x)$.

5. Numerical results. In this section we present a numerical scheme for solving the hybrid stochastic Fokker–Planck–Boltzmann traffic equation (4.6) along the lines of UQ. Among the popular numerical methods in the literature for UQ we recall here in particular stochastic collocation methods, stochastic Galerkin schemes, and multilevel Monte Carlo methods; see, e.g., [15, 32, 53]. In what follows we will specifically consider stochastic collocation methods. They are based on introducing a discretization $\{\theta_k\}_{k=0}^M \subset I_\Theta$ of the uncertain parameter θ and then in solving, by means of well-established deterministic algorithms, a family of $M+1$ equations of the form (4.6), each for a fixed value $\theta = \theta_k$. Their solutions $\{g(\mathbf{v},\, \tau;\, \theta_k)\}_{k=0}^M$ can finally be postprocessed to obtain statistical information at both the kinetic and the macroscopic level with respect to θ; cf. section 3. The collocation nodes θ_k are typically chosen according to Gaussian quadrature rules and consistently with the probability distribution of θ; see [52, 54].

As a preliminary step to the numerical solution of (4.6), we consider the following dimensional splitting: on a certain time interval $[\tau^n,\, \tau^{n+1}]$ with $\tau^n := n\Delta\tau$, $n \in \mathbb{N}$, and $\Delta\tau > 0$ fixed, we first solve the Fokker–Planck step in $(\tau^n,\, \tau^{n+1/2}]$:

$$\begin{cases} \partial_\tau \tilde{g} = \partial_{v_x} \left(\mathcal{L}[\tilde{g}]\tilde{g} + \dfrac{\sigma^2}{2} \partial_{v_x}(\mathcal{D}[\tilde{g}]\tilde{g}) \right), \quad v_x \in \mathbb{V}_x,\ \tau^n < \tau \leq \tau^{n+1/2}, \\ \tilde{g}(\mathbf{v},\, \tau^n;\, \theta) = g(\mathbf{v},\, \tau^n;\, \theta) \end{cases} \tag{5.1}$$

for all $v_y \in \mathbb{V}_y$ (regarded as a parameter) with the nonlocal operators $\mathcal{L}[\cdot]$, $\mathcal{D}[\cdot]$ defined as in (4.3) and (4.5); we refer the reader to Table 2 for the definitions of all the relevant quantities concurring with the definitions of these operators. To help the reader, we report here the explicit expressions of the operators that we consider in the forthcoming numerical tests:

$$\mathcal{L}[\tilde{g}] = \frac{\rho}{2} \int_{\mathbb{V}} L(v_x, \min\{v_x + \Delta v, 1\}, P(\rho)w_x, w_x)\tilde{g}(\mathbf{w}, \tau; \theta) d\mathbf{w},$$
$$\mathcal{D}[\tilde{g}] = \frac{\rho}{2} \int_{\mathbb{V}} D^2(v_x, w_x)\tilde{g}(\mathbf{w}, \tau; \theta) d\mathbf{w},$$

TABLE 2
Summary of the main parameters used in the numerical simulations.

Parameter	Value
W_x	w_x
$P(\rho)$	$1-\rho$
V_A	$\min\{v_x+\Delta v,\,1\}$
V_B	$P(\rho)W_x$
Δv	0.2

being

$$L(v_x,\min\{v_x+\Delta v,1\},P(\rho)w_x,w_x)$$
$$=\begin{cases}P(\rho)(v_x-\min\{v_x+\Delta v,1\}) & \text{if } v_x<w_x,\\ (1-P(\rho))(v_x-P(\rho)w_x)\text{if} & \text{if } v_x>w_x,\end{cases}$$
$$D(v_x,w_x)$$
$$=\begin{cases}\sqrt{P(\rho)}\nu(v_x)(\min\{v_x+\Delta v,1\}-v_x) & \text{if } v_x<w_x,\\ \sqrt{1-P(\rho)}\nu(v_x)(v_x-P(\rho)w_x) & \text{if } v_x>w_x.\end{cases}$$

Next, in $(\tau^{n+1/2},\tau^{n+1}]$ we solve the Boltzmann step as

$$\begin{cases}\partial_\tau g=\mu\rho Q_y(g), & v_y\in\mathbb{V}_y,\ \tau^{n+1/2}<\tau\le\tau^{n+1},\\ g(\mathbf{v},\,\tau^{n+1/2};\,\theta)=\tilde g(\mathbf{v},\,\tau^{n+1/2};\,\theta)\end{cases}\tag{5.2}$$

for all $v_x\in\mathbb{V}_x$ (regarded as a parameter). This process may be iterated to obtain the numerical solution of the initial equation at each time step.

To approximate numerically (5.1) we adopt SP methods which have been recently developed in [39]; see also [15, 47]. Conversely, to solve (5.2) we use direct Monte Carlo methods; see, e.g., [35, 36]. In particular, we employ stratified sampling methods to extract at each time step from $\tilde g$ the particle ensemble to be evolved in (5.2); see [34].

5.1. Structure preserving methods for nonlinear Fokker–Planck equations. The derivation of SP schemes in the fully nonlinear case (i.e., for a Fokker–Planck equation in which the diffusion coefficient depends on the unknown distribution function itself) follows from the approaches described in [7, 10, 30] and has been further investigated, in both the deterministic and stochastic settings, in the recent works [15, 39].

We observe that for each θ_k, $k=0,\dots,M$, the Fokker–Planck equation in (5.1) may be written in flux form

$$\partial_\tau\tilde g(\mathbf{v},\,\tau;\,\theta_k)=\partial_{v_x}\mathcal{F}[\tilde g](\mathbf{v},\,\tau;\,\theta_k),$$

where the flux is

$$\mathcal{F}[\tilde g](\mathbf{v},\,\tau;\,\theta_k):=\mathcal{C}[\tilde g](\mathbf{v},\,\tau;\,\theta_k)\tilde g(\mathbf{v},\,\tau;\,\theta_k)+\frac{\sigma^2}{2}\mathcal{D}[\tilde g](\mathbf{v},\,\tau;\,\theta_k)\partial_{v_x}\tilde g(\mathbf{v},\,\tau;\,\theta_k)\tag{5.3}$$

with $\mathcal{C}[\tilde g]:=\mathcal{L}[\tilde g]+\partial_{v_x}\mathcal{D}[\tilde g]$ and $\mathcal{L}$, $\mathcal{D}$ are defined in (4.5).

We introduce the uniform grids $\{v_{x,i}\}_{i=1}^{N_x}\subset\mathbb{V}_x$, $\{v_{y,j}\}_{j=1}^{N_y}\subset\mathbb{V}_y$ and let $\Delta v_x:=v_{x,i+1}-v_{x,i}>0$. In the rest of this section, for ease of notation, we drop the index

j since v_y remains constant in the Fokker–Planck step (5.1). We denote as usual $v_{x,i+1/2} := v_{x,i} + \frac{1}{2}\Delta v_x$ and consider the conservative discretization

$$\frac{d}{d\tau}\tilde{g}_i^k(\tau) = \frac{\mathcal{F}_{i+1/2}^k[\tilde{g}] - \mathcal{F}_{i-1/2}^k[\tilde{g}]}{\Delta v_x}, \qquad i = 1, \dots, N_x, \tag{5.4}$$

where, for each $\tau > 0$, $\tilde{g}_i^k(\tau) \approx \tilde{g}(v_{x,i}, v_y, \tau; \theta_k)$ while $\mathcal{F}_{i+1/2}^k[\tilde{g}]$ is the numerical flux that here we take of the form (cf. (5.3))

$$\mathcal{F}_{i+1/2}^k[\tilde{g}] = \hat{\mathcal{C}}_{i+1/2}^k \hat{g}_{i+1/2}^k + \frac{\sigma^2 \mathcal{D}_{i+1/2}^k}{2} \frac{\tilde{g}_{i+1}^k - \tilde{g}_i^k}{\Delta v_x}. \tag{5.5}$$

In (5.5) we set in particular

$$\hat{g}_{i+1/2}^k := \left(1 - \delta_{i+1/2}^k\right) \tilde{g}_{i+1}^k + \delta_{i+1/2}^k \tilde{g}_i^k,$$

which is a convex combination of the values of $\tilde{g}^k$ in the two adjacent cells i, $i+1$ provided $0 \le \delta_{i+1/2}^k \le 1$. The standard approach based on central difference is obtained taking $\delta_{i+1/2}^k = \frac{1}{2}$ for all i and $\hat{\mathcal{C}}_{i+1/2}^k := \mathcal{C}[\tilde{g}](v_{x,i+1/2}, v_y, \tau; \theta_k)$. It is worth pointing out that a numerical scheme based on central difference imposes stability restrictions on Δv_x. On the contrary, the present approach permits us to derive bounds on the time step. Setting in particular

$$\hat{\mathcal{C}}_{i+1/2}^k = \mathcal{L}_{i+1/2}^k + \frac{\sigma^2}{2}(\partial_{v_x}\mathcal{D})_{i+1/2}^k \tag{5.6}$$

we obtain explicitly

$$\delta_{i+1/2}^k = \frac{1}{\lambda_{i+1/2}^k} + \frac{1}{1 - \exp(\lambda_{i+1/2}^k)}, \qquad \lambda_{i+1/2}^k := \frac{2\Delta v_x \hat{\mathcal{C}}_{i+1/2}^k}{\sigma^2 \mathcal{D}_{i+1/2}^k}, \tag{5.7}$$

and the following result holds (cf. [39]).

PROPOSITION 3. *The numerical flux* (5.5) *with* $\hat{\mathcal{C}}_{i+1/2}^k$, $\delta_{i+1/2}^k$ *given by* (5.6)–(5.7) *vanishes when the exact flux* (5.3) *vanishes in* $[v_{x,i}, v_{x,i+1}] \subset \mathbb{V}_x$. *Moreover,* $\delta_{i+1/2}^k \in [0, 1]$ *for all* i *and for every fixed* j, k.

Remark 3. In the limit case of vanishing diffusion ($\mathcal{D} = 0$) we obtain the weights

$$\delta_{i+1/2}^k = \begin{cases} 0 & \text{if } \mathcal{L}_{i+1/2}^k > 0, \\ 1 & \text{if } \mathcal{L}_{i+1/2}^k < 0, \end{cases}$$

and the scheme reduces to a first order upwind scheme for the corresponding diffusionless mean-field type equation.

The introduced scheme preserves the asymptotic solutions of the Fokker–Planck equation in (5.1) with second order accuracy. In the case of linear diffusion, i.e., for $\mathcal{D}$ independent of $\tilde{g}$, it captures such solutions with arbitrary accuracy; see [15, 39]. Furthermore, for general strong stability preserving and high order semi-implicit methods it is possible to prove the nonnegativity of the numerical solution without any restrictions on Δv_x but with suitable restrictions on the time step $\Delta\tau$.

For the explicit-in-time scheme deduced from (5.4), i.e.,

$$\tilde{g}_i^{k,n+1/2} = \tilde{g}_i^{k,n} + \frac{\Delta\tau}{\Delta v_x}\left(\mathcal{F}_{i+1/2}^{k,n}[\tilde{g}] - \mathcal{F}_{i-1/2}^{k,n}[\tilde{g}]\right),$$

where $\tilde{g}_i^{k,n} \approx \tilde{g}(v_{x,i}, v_y, n\Delta\tau; \theta_k)$, the following result holds.

PROPOSITION 4. *Let*

$$\Delta\tau \le \frac{\Delta v_x^2}{2\left(\max\limits_{i,k}|\hat{\mathcal{C}}_{i+1/2}^k|\Delta v_x + \max\limits_{i,k}\mathcal{D}_{i+1/2}^k\right)}.$$

Then the explicit-in-time scheme is positivity preserving, i.e., $\tilde{g}_i^{k,n+1/2} \ge 0$ *if* $\tilde{g}_i^{k,n} \ge 0$ *for all* i, j.

To avoid parabolic time step restrictions typical of the explicit schemes, such as the one in Proposition 4, it is possible to resort to a semi-implicit scheme:

$$\tilde{g}_i^{k,n+1/2} = \tilde{g}_i^{k,n} + \frac{\Delta\tau}{\Delta v_x}\left(\check{\mathcal{F}}_{i+1/2}^{k,n+1/2}[\tilde{g}] - \check{\mathcal{F}}_{i-1/2}^{k,n+1/2}[\tilde{g}]\right)$$

with

$$\check{\mathcal{F}}_{i+1/2}^{k,n+1/2} := \hat{\mathcal{C}}_{i+1/2}^{k,n}\left[\left(1-\delta_{i+1/2}^{k,n}\right)\tilde{g}_{i+1}^{k,n+1/2} + \delta_{i+1/2}^{k,n}\tilde{g}_i^{k,n+1/2}\right] + \frac{\sigma^2\mathcal{D}_{i+1/2}^n}{2}\frac{\tilde{g}_{i+1}^{k,n+1/2} - \tilde{g}_i^{k,n+1/2}}{\Delta v_x}.$$

In this case the following result holds.

PROPOSITION 5. *Let*

$$\Delta\tau \le \frac{\Delta v_x}{2\max\limits_{i,k}|\hat{\mathcal{C}}_{i+1/2}^{k,n}|}.$$

Then the semi-implicit scheme is positivity preserving.

We omit the proofs of Propositions 4, 5, which are reminiscent of similar ones proposed in [39].

In order to show the effectiveness of the described scheme we now apply it to the nonlinear Fokker–Planck equation in (5.1) with $W_x = w_x$ and V_A, V_B like in (2.3). Notice that, since in this illustrative example we are not interested in the coupling with (5.2), we can formally neglect the variables v_y, θ, thereby reducing the problem to a one-dimensional equation in the sole variable v_x.

In Figure 1 we show the stationary profiles of the kinetic distribution for $\rho = 0.3, 0.5, 0.7$ and two choices of the diffusion constant $\sigma^2 = 10, 15$. The profiles of the densities for large times ($T = 10^3$) have been obtained via the semi-implicit SP scheme for the nonlinear Fokker–Planck equation with $\Delta\tau = \Delta v_x/\sigma^2$.

Furthermore, in Table 3 we estimate the order of convergence of the semi-implicit SP scheme for $\rho = 0.3, 0.7$ and $\sigma^2 = 15$ as $\log_2 \frac{e_1(\tau)}{e_2(\tau)}$, where $e_1(\tau)$ is the relative error at time τ of the solution computed with $N_x = 21$ grid points with respect to that computed with $N_x = 41$ grid points and, likewise, $e_2(\tau)$ is the relative error at time τ of the solution computed with $N_x = 41$ grid points with respect to that computed with $N_x = 81$ grid points. The time step is such that the CFL condition for the positivity of the scheme is satisfied, i.e., $\Delta\tau = O(\Delta v_x)$ in the semi-implicit case according to Proposition 5.

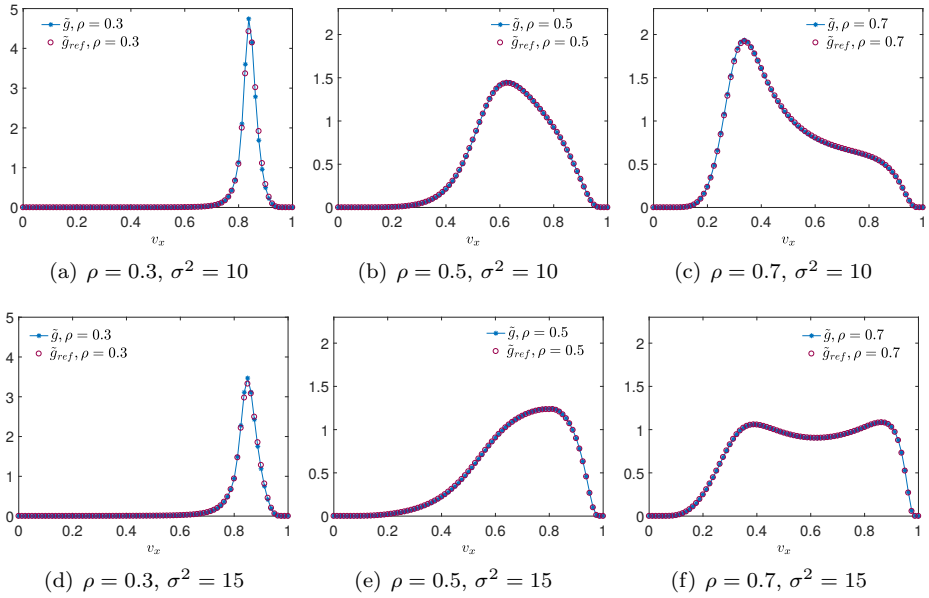

(a) $\rho = 0.3$, $\sigma^2 = 10$ (b) $\rho = 0.5$, $\sigma^2 = 10$ (c) $\rho = 0.7$, $\sigma^2 = 10$

(d) $\rho = 0.3$, $\sigma^2 = 15$ (e) $\rho = 0.5$, $\sigma^2 = 15$ (f) $\rho = 0.7$, $\sigma^2 = 15$

FIG. 1. *Large time solutions of the Fokker–Planck equation in* (5.1) *computed with the semi-implicit SP scheme for the values of* $\rho = 0.3, 0.5, 0.7$ *and* $\sigma^2 = 10, 15$, $\Delta\tau = \Delta v_x/\sigma^2$, *and final time* $T = 10^3$. *The blue line is the solution computed with* $N_x = 41$ *grid points while the red circles represent the reference solution computed with* $N_x = 321$ *grid points. See Table 2 for the specific choice of the model parameters necessary for the definition of the SP scheme. We considered as an initial distribution* $\tilde{g}_0(v_x) = \chi_{[0,1]}(v_x)$.

TABLE 3
Estimate of the order of convergence of the semi-implicit SP scheme for the Fokker–Planck equation in (5.1) *with* $\sigma^2 = 15$ *and* $\Delta\tau = \Delta v_x/\sigma^2$.

	$\rho = 0.3$	$\rho = 0.7$
$\tau = 1$	1.7543	1.7794
$\tau = 20$	1.9524	1.7821
$\tau = 60$	2.2934	1.9282
$\tau = 100$	2.3014	1.9283

5.2. The two-dimensional stochastic model. We now turn to the numerical solution of the two-dimensional hybrid stochastic model (4.6) by means of the dimensional splitting illustrated at the beginning of section 5. We consider as an initial condition the following deterministic distribution:

$$g(\mathbf{v}, 0; \theta) = g_0(\mathbf{v}) = g_{0,x}(v_x)g_{0,y}(v_y), \tag{5.8}$$

which does not depend on the random parameter θ, with in particular

$$g_{0,x}(v_x) = \chi_{[0,1]}(v_x), \qquad g_{0,y}(v_y) = \frac{1}{2}\chi_{[-1,1]}(v_y). \tag{5.9}$$

Notice that the choice of $g_{0,y}$ implies that we are fixing $\mathbb{V}_y = [-1, 1]$, i.e., $\varepsilon = 1$.

As far as the random input θ is concerned, we choose $\theta \sim \mathcal{U}(-1, 1)$, and hence $I_\Theta = [-1, 1]$ and $h(\theta) = \frac{1}{2}\chi_{[-1,1]}(\theta)$, and a desired speed in (2.7) of the form

$$v_d(\theta) = \bar{v}_d + \lambda P(\rho)\theta, \tag{5.10}$$

where $\bar{v}_d \in (-1, 1)$ and $\lambda > 0$ are given constants. For the application of the stochas-

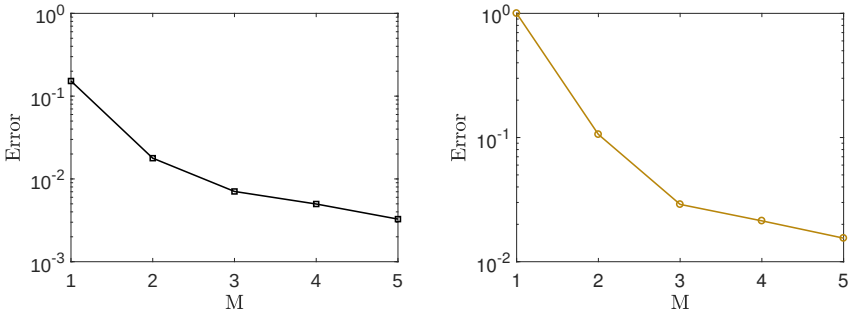

FIG. 2. *Average relative L^1 error on the θ-expected solution (left) and its θ-variance (right) of* (4.6) *via the dimensional splitting* (5.1)–(5.2) *for an increasing number $M = 1, \dots, 5$ of collocation nodes in I_Θ taking $\theta \sim \mathcal{U}([-1, 1])$. The reference numerical solution is computed with $M = 50$ collocation nodes. In* (5.10) *we have fixed $\bar{v}_d = 0$ and $\lambda = 10^{-1}$. Moreover, we have fixed $T = 10^2$, $\Delta\tau = \Delta v_x/\sigma^2$, $\mu = 1$, $\sigma^2 = 10$ and we have discretized the velocity space with $N_x = 101$ and $N_y = 41$ grid points. The relaxation rate in* (2.7) *is $\beta(u_x) = u_x$. We considered the deterministic initial distribution given in* (5.8)–(5.9).

tic collocation method we discretize θ by means of the first $M > 1$ Gauss–Legendre collocation nodes.

Finally, we solve the Boltzmann step (5.2) via a direct Monte Carlo method implemented through the Nanbu algorithm [6]. Precisely, we use $N = 10^4$ y-speeds extracted from the distribution $\tilde{g}$ with a stratified sampling approach [34] and we approximate the collisional equation in (5.2) as

$$g^{n+1} = (1 - \mu\rho\Delta\tau)g^{n+1/2} + \mu\rho\Delta\tau Q_y^+\left(g^{n+1/2}\right), \tag{5.11}$$

where $Q_y^+(g) := \frac{1}{1-\beta(u_x)} g('\mathbf{v}_y, \tau; \theta)$ is the *gain* term of the collision operator Q_y. Observing that $Q_y^+(g)$ is a probability distribution, we see that under the restriction $\mu\rho\Delta\tau \leq 1$ the previous equation is a convex combination of the probability distributions $g^{n+1/2}$ and $Q_y^+(g^{n+1/2})$, and therefore also g^{n+1} is a probability density function. The probabilistic interpretation of (5.11), which underlies the direct Monte Carlo method used for the numerical solution, is the following: a vehicle with lateral speed v_y will not interact with other vehicles with probability $1 - \mu\rho\Delta\tau$ while it will interact with probability $\mu\rho\Delta\tau$ according to the interaction law defined by $Q_y^+(g^{n+1/2})$.

In Figure 2 we show the relative L^1 error on the expected solution $\bar{g}$ and its variance $\mathrm{Var}_\theta(g)$ (cf. (3.2)), of the full two-dimensional problem for an increasing number $M = 1, \dots, 5$ of collocation nodes in I_Θ, computed with respect to a reference numerical solution on $M = 50$ nodes. The variable v_x has been discretized with $N_x = 101$ grid points in $\mathbb{V}_x$, the variable v_y with $N_y = 41$ grid points in $\mathbb{V}_y$, and a time step $\Delta\tau = O(\Delta v_x)$ has been chosen for the semi-implicit SP scheme (cf. Proposition 5) with final time $T = 100$. We point out that, due to the stratified sampling approach, the curves plotted in Figure 2 are actually averages computed out of 10^2 estimates of the relative error.

In Figures 3 and 4 we show instead the time evolution of the expected solution $\bar{g}$ and of its variance $\mathrm{Var}_\theta(g)$, respectively (cf. again (3.2)) for the traffic densities $\rho = 0.3, 0.6, 0.9$. In particular, the graphs of $\mathrm{Var}_\theta(g)$ highlight the regions of the space of the microscopic states $\mathbb{V} = \mathbb{V}_x \times \mathbb{V}_y$, where the statistical variability of the expected solution $\bar{g}$ is higher due to the uncertainty in $v_d(\theta)$ of the form introduced in (5.10).

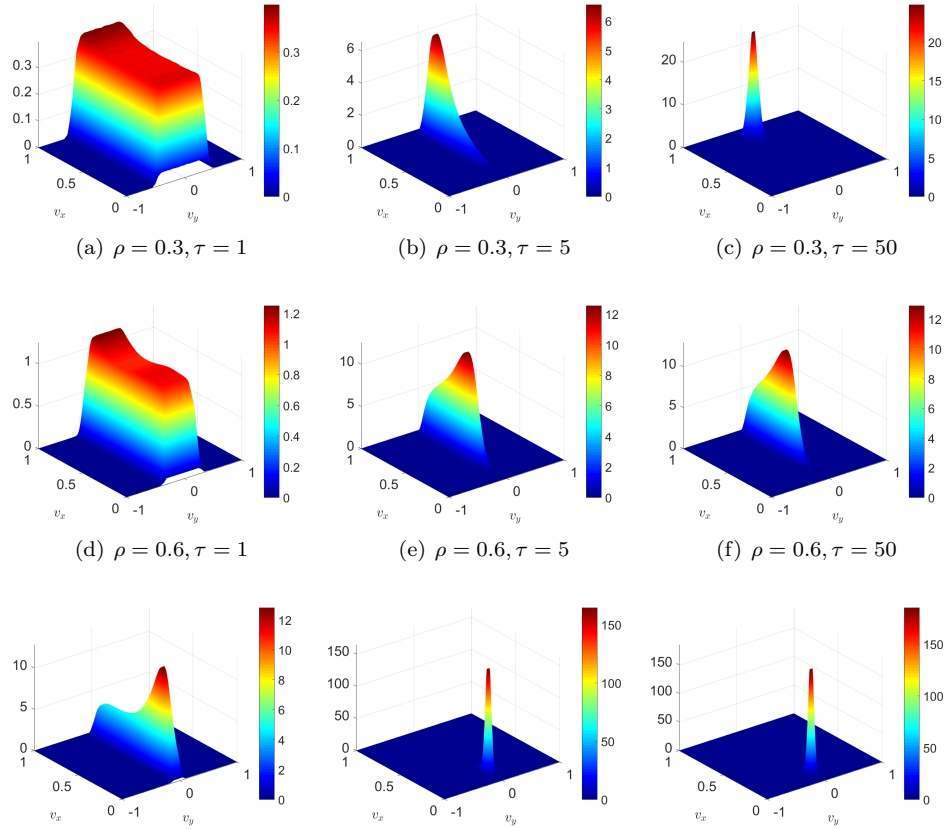

(a) $\rho = 0.3, \tau = 1$ (b) $\rho = 0.3, \tau = 5$ (c) $\rho = 0.3, \tau = 50$

(d) $\rho = 0.6, \tau = 1$ (e) $\rho = 0.6, \tau = 5$ (f) $\rho = 0.6, \tau = 50$

(g) $\rho = 0.9, \tau = 1$ (h) $\rho = 0.9, \tau = 5$ (i) $\rho = 0.9, \tau = 50$

FIG. 3. *Evolution of the θ-expected solution of* (4.6) *for different values of the traffic density, in particular $\rho = 0.3$ (top row), $\rho = 0.6$ (middle row), and $\rho = 0.9$ (bottom row). The collocation method for the UQ has been implemented taking $\theta \sim \mathcal{U}([-1, 1])$ and using $M = 5$ nodes in the interval $[-1, 1]$. We have considered $v_d(\theta)$ of the form* (5.10) *with $\bar{v}_d = 0$, $\lambda = 10^{-1}$, $\Delta\tau = \Delta v_x/\sigma^2$, $\sigma^2 = 10$, $\mu = 1$ and we have discretized the velocity space with $N_x = 101$, $N_y = 41$ grid points. We considered the deterministic initial distribution given in* (5.8)–(5.9).

5.3. Two-dimensional speed diagrams of traffic. A usual benchmark for validating a kinetic traffic model consists in checking if the theoretical speed diagrams arising from the asymptotic kinetic distributions reproduce the features typically observed in the empirical speed diagrams.

Speed diagrams express the average speed of the vehicles as a function of the vehicle density at equilibrium and in spatially homogeneous conditions. In our case, we compute the mean speeds at equilibrium from the asymptotic solution of (4.6) as

$$u_x^\infty = \int_{\mathbb{V}} v_x g^\infty(\mathbf{v};\, \theta)\, d\mathbf{v} = \int_0^1 v_x g_x^\infty(v_x)\, dv_x,$$
$$u_y^\infty(\theta) = \int_{\mathbb{V}} v_y g^\infty(\mathbf{v};\, \theta)\, d\mathbf{v} = \int_{-\varepsilon}^{\varepsilon} v_y g_y^\infty(v_y;\, \theta)\, dv_y.$$

Notice that only the asymptotic y-mean speed is actually uncertain, because the y-dynamics (2.7) contain the random input θ. The asymptotic x-mean speed is not,

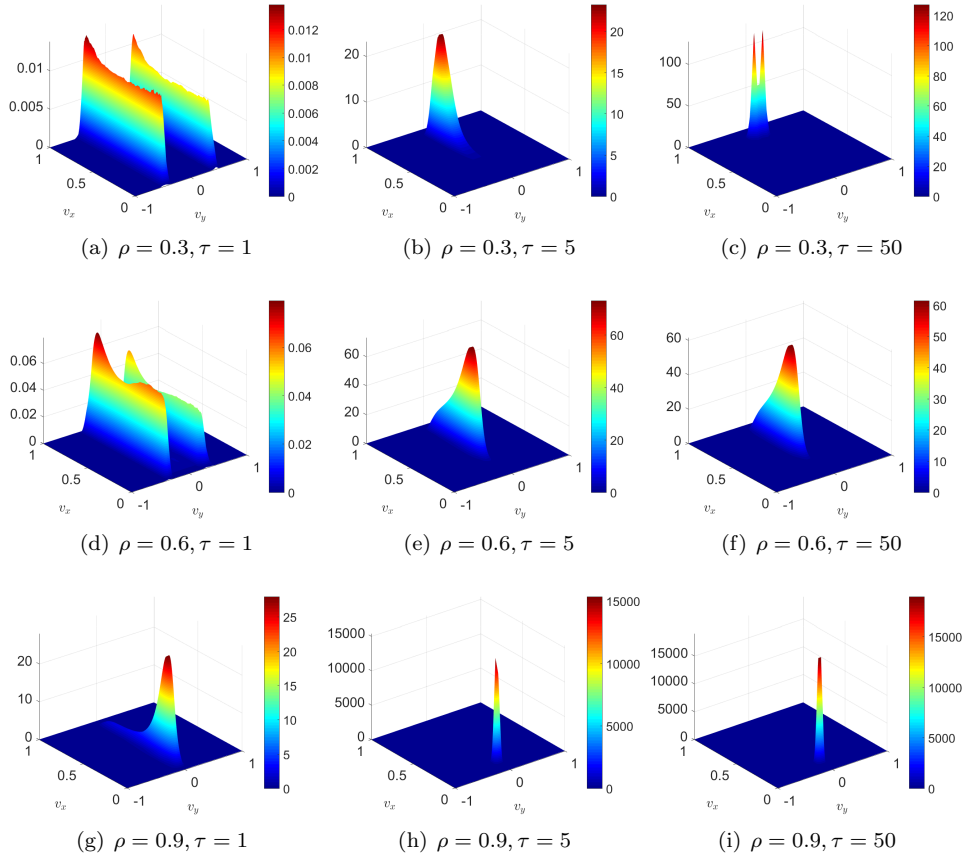

(a) $\rho = 0.3, \tau = 1$ (b) $\rho = 0.3, \tau = 5$ (c) $\rho = 0.3, \tau = 50$

(d) $\rho = 0.6, \tau = 1$ (e) $\rho = 0.6, \tau = 5$ (f) $\rho = 0.6, \tau = 50$

(g) $\rho = 0.9, \tau = 1$ (h) $\rho = 0.9, \tau = 5$ (i) $\rho = 0.9, \tau = 50$

FIG. 4. *Evolution of the θ-variance of the expected solution to* (4.6) *for different values of the traffic density, in particular $\rho = 0.3$ (top row), $\rho = 0.6$ (middle row), and $\rho = 0.9$ (bottom row). The collocation method for the UQ has been implemented taking $\theta \sim \mathcal{U}([-1, 1])$ and using $M = 5$ nodes in the interval $[-1, 1]$. We have considered $v_d(\theta)$ of the form* (5.10) *with $\bar{v}_d = 0$, $\lambda = 10^{-1}$, $\Delta\tau = \Delta v_x/\sigma^2$, $\sigma^2 = 10$, $\mu = 1$ and we have discretized the velocity space with $N_x = 101$, $N_y = 41$ grid points. We considered the deterministic initial distribution given in* (5.8)–(5.9).

because the x-dynamics (2.1a)–(2.1b) do not contain any random input nor any explicit coupling with the y-dynamics. By further averaging u_y^∞ with respect to the uncertainty in θ we get

$$\bar{u}_y^\infty := \int_{I_\Theta} u_y^\infty(\theta) h(\theta)\, d\theta,$$

while obviously it results in $\bar{u}_x^\infty = u_x^\infty$. Clearly, these values depend on the density $\rho \in [0, 1]$ fixed in (4.3), hence in (4.5), and in (4.6). Finally, we plot the mappings $\rho \mapsto \bar{u}_y^\infty$, $\rho \mapsto u_x^\infty$ and compare them with the empirical ones obtained from a dataset described below; cf. section 5.3.1.

In order to reproduce the scattering of the experimental data normally seen in the measured speed diagrams, we compute the following indicator of maximum dispersion of the y-energy:

$$I_y := \bar{E}_y^\infty + \sqrt{\mathrm{Var}_\theta(E_y^\infty)},$$

where $\bar{E}_y^\infty$ denotes the θ-expected value of the asymptotic energy in the y-direction

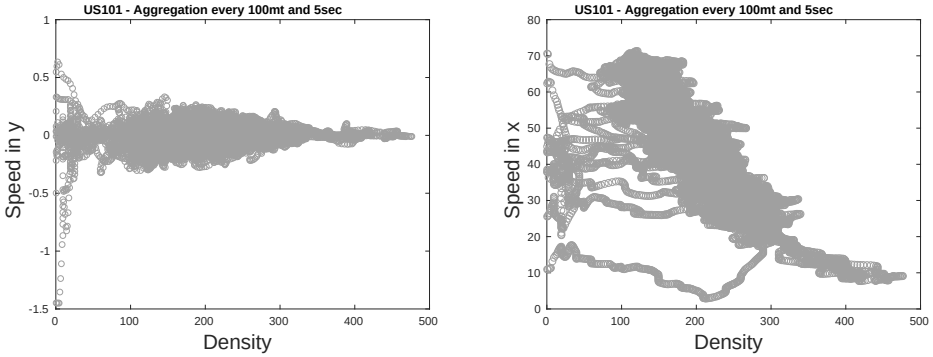

(a) (b)

FIG. 5. *Speed-density diagrams in the y-direction* (a) *and x-direction* (b). *The grey circles are the experimental speeds obtained from the U.S. dataset described in section* 5.3.1.

and $\mathrm{Var}_\theta(E_y^\infty)$ its θ-variance, then we plot the mappings $\rho \mapsto \bar{u}_y^\infty \pm \sqrt{I_y}$. Notice that I_y represents the deviation from the expected y-energy of the model, and hence its square root is dimensionally comparable to a speed.

5.3.1. Experimental dataset. We consider a set of experimental data recorded on a section on the southbound direction of the U.S. Highway 101 (known as Hollywood Freeway) in Los Angeles, California. The data are part of the Federal Highway Administration's Next Generation Simulation project [1]. They consist of the two-dimensional vehicle trajectories collected between 7:50 am and 8:15 am on June 15, 2005 using 8 video cameras with a resolution of 10 frames per second. The road section is approximately 640 m in length with five main lanes plus an auxiliary lane in the corridor between an incoming and an outgoing ramp. However, we only consider the stretch as if there were no ramps.

The microscopic velocities of the vehicles are recovered out of their microscopic positions in consecutive frames. From the microscopic data, the macroscopic quantities in each direction of the flow can be computed as explained, e.g., in [24, 31]. The aggregation of the data is made with respect to time (5 s) and distance (100 m).

In Figure 5 we observe that the order of magnitude of the recorded mean speed in the y-direction is much smaller than that in the x-direction, which indeed justifies the formulation of a hybrid kinetic model to clearly separate the two speed scales. We stress that, to our knowledge, this is one of the first times that speed diagrams are recorded also for lateral displacements of the cars across the lanes.

5.3.2. Theoretical speed diagrams. In Figure 6 we show the theoretical speed-density diagrams, computed as discussed at the beginning of section 5.3, in both the y-direction (a) and the x-direction (b). For straightforward comparison, we place them on top of the empirical data (grey circles), which here are duly normalized with respect to the maximum density and the maximum speed in either direction of the flow for consistency with the dimensionless results of the mathematical model.

The red solid lines are the graphs of the mappings $\rho \mapsto \bar{u}_y^\infty$ in Figure 6(a) and $\rho \mapsto u_x^\infty$ in Figure 6(b). The black dashed lines in Figure 6(a) are instead the graphs of the mappings $\rho \mapsto \bar{u}_y^\infty \pm \sqrt{I_y}$. On the whole, we see that the theoretical results reproduce quite well the measurements. In particular, we notice that the theoretical speed diagram in the y-direction is constant at all densities around the value $\bar{v}_d$

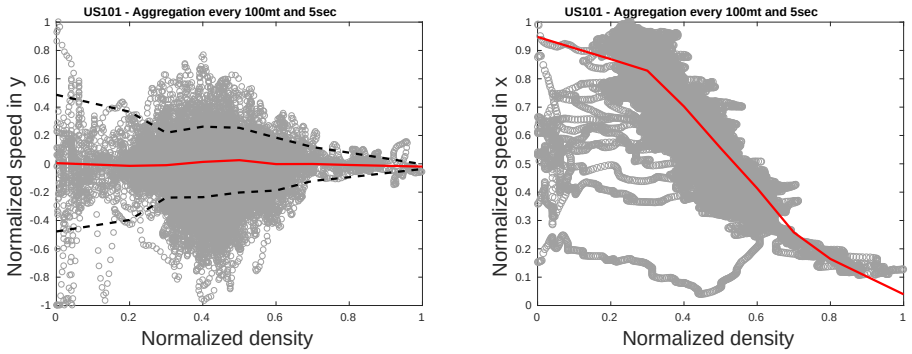

(a) (b)

FIG. 6. *Theoretical speed-density diagrams (red, black lines) in the y-direction* (a) *and the x-direction* (b) *on top of the normalized empirical ones (grey circles). The red solid lines are the θ-expected asymptotic mean speeds in the two directions of the flow while the black dashed lines in* (a) *are the deviations from the mean speed* $\bar{u}_y^\infty$ *given by the energy-based estimator* I_y. *In* (5.10) *we have set* $\bar{v}_d = -0.0109$ *and* $\lambda = \frac{1}{2}$.

in (5.10), which here we set to $\bar{v}_d = -0.0109$ (estimated from the data). In contrast, the theoretical speed diagram in the x-direction shows the typical decreasing trend toward zero at high density (congested traffic phase) after a nearly constant trend for low density (free traffic phase).

As far as the data scattering is concerned, we observe that the energy-based confidence interval around $\bar{u}_y^\infty$ estimated by means of I_y (cf. Figure 6(a)) catches the qualitative trend of the empirical speed values, thus suggesting that the data dispersion in the y-direction can be indeed explained in terms of the stochastic variability due to θ in the microscopic dynamics across the lanes; cf. (2.7), (5.10). Again, we stress that, to our knowledge, this is one of the first times that theoretical speed diagrams due to lane changes are studied and explained by a mathematical model. Since we have not included any source of uncertainty in the x-dynamics (2.1a)–(2.1b), we cannot reproduce a similar estimate of the data dispersion in the theoretical x-speed diagram. However, for the sake of completeness, we mention that other works offer alternative explanations for the data dispersion in the x-direction which do not appeal to uncertain parameters nor UQ; see, e.g., [17, 43, 51].

Thanks to the results of section 4.2, we can also compute analytically the theoretical curves appearing in the y-speed diagram of Figure 6(a). In fact from $g_y^\infty(v_y;\, \theta) = \delta_{v_d(\theta)}(v_y)$ we have $u_y^\infty(\theta) = v_d(\theta)$, whence using (5.10) with $\theta \sim \mathcal{U}(-1,\, 1)$ we obtain

$$\bar{u}_y^\infty = \frac{1}{2}\int_{-1}^{1} v_d(\theta)\, d\theta = \bar{v}_d,$$

which is the equation of the red line in Figure 6(a). Moreover, since $E_y^\infty(\theta) = v_d^2(\theta)$ we compute

$$\bar{E}_y^\infty(\theta) = \frac{1}{2}\int_{-1}^{1} v_d^2(\theta)\, d\theta = \bar{v}_d^2 + \frac{1}{3}\lambda^2 P^2(\rho),$$

$$\mathrm{Var}_\theta(E_y^\infty) = \frac{1}{2}\int_{-1}^{1} v_d^4(\theta)\, d\theta - \left(\bar{E}_y^\infty\right)^2 = 4\left(\frac{1}{3}\bar{v}_d^2 + \frac{1}{45}\lambda^2 P^2(\rho)\right)\lambda^2 P^2(\rho).$$

In particular, for $\bar{v}_d = 0$ (nearly the value used for the simulated diagram of Figure 6(a)) this gives $I_y = (\frac{1}{3} + \frac{2}{\sqrt{45}})\lambda^2 P^2(\rho)$, and thus the curves of the energy-based

confidence interval in the y-speed diagram are

$$\bar{u}_y^\infty \pm \sqrt{I_y} = \pm\sqrt{\frac{1}{3} + \frac{2}{\sqrt{45}}}\lambda P(\rho) \approx \pm 0.4(1-\rho)$$

for the expression (2.2) of $P(\rho)$ with the value of λ in Figure 6(a).

6. Conclusion. In this work we have introduced a hybrid stochastic kinetic model of two-dimensional traffic dynamics, which takes into account speed changes both along and across road lanes as a consequence of vehicle interactions and lane changes, respectively. Starting from a Boltzmann-type description based on suitable microscopic dynamics, we have derived a hybrid Fokker–Planck–Boltzmann equation in the quasi-invariant interaction limit assuming that lane changes, described by a linear collision operator, are much less frequent than speed variations along the lanes, described by a nonlinear Fokker–Planck operator. In particular, we have suggested that speed variations due to lane changes can be modeled at the microscopic level simply as a relaxation process toward a desired lateral speed, which however is not known deterministically. This introduces an intrinsic uncertainty in the kinetic equation, which proves to be essential for reproducing theoretically not only the average macroscopic trends observed in reality but also the scattering of the experimental data typical of the empirical fundamental diagrams of traffic.

Besides the result just mentioned, the main methodological contributions of this work are the following: (i) we have proposed a formal asymptotic procedure to derive hybrid kinetic models including uncertain parameters, which can be applied to multivariate microscopic dynamics when some of them occur at a much lower rate than others. The advantage is that the most frequent dynamics turn out to be modeled by Fokker–Planck-type differential operators replacing the original Boltzmann-type collision operators, while the latter remain to model only the less frequent dynamics; (ii) we have proposed a numerical study of the general hybrid stochastic kinetic equation by means of an extension of SP methods existing in the literature to fully nonlinear Fokker–Planck equations combined with direct Monte Carlo methods, stratified sampling, and UQ collocation methods to quantify the uncertainty intrinsic in the stochastic kinetic equation.

Further amplifications of the present work may include a systematic study of the numerical method for the hybrid kinetic equation with special attention to the case of possibly vanishing nonlinear diffusion in the Fokker–Planck operator. From the modeling point of view, the derivation of macroscopic traffic equations in a suitable hydrodynamic limit from the hybrid stochastic kinetic description is another completely open issue.

Acknowledgments. A. T. is member of GNFM (Gruppo Nazionale per la Fisica Matematica) of INdAM (Istituto Nazionale di Alta Matematica), Italy. G. V. and M. Z. are members of GNCS (Gruppo Nazionale per il Calcolo Scientifico) of INdAM, Italy.

REFERENCES

[1] Federal Highway Administration U.S. Department of Transportation, *Next Generation Simulation (NGSIM)*, http://ops.fhwa.dot.gov/trafficanalysistools/ngsim.htm.

[2] J. P. Agnelli, F. Colasuonno, and D. Knopoff, *A kinetic theory approach to the dynamics of crowd evacuation from bounded domains*, Math. Models Methods Appl. Sci., 25 (2015), pp. 109–129.

[3] G. Albi, L. Pareschi, G. Toscani, and M. Zanella, *Recent advances in opinion modeling: Control and social influence*, in Active Particles Volume 1, Theory, Methods, and Applications, N. Bellomo, P. Degond, and E. Tadmor, eds., Model. Simul. Sci. Eng. Technol., Birkhäuser, Boston, 2016.

[4] G. Albi, L. Pareschi, and M. Zanella, *Uncertainty quantification in control problems for flocking models*, Math. Probl. Eng., 2015 (2015), 850124.

[5] M. Ballerini, N. Cabibbo, R. Candelier, A. Cavagna, E. Cisbani, I. Giardina, A. Orlandi, G. Parisi, A. Procaccini, M. Viale, and V. Zdravkovic, *Empirical investigation of starling flocks: A benchmark study in collective animal behaviour*, Anim. Behav., 76 (2008), pp. 201–215.

[6] A. V. Bobylev and K. Nanbu, *Theory of collision algorithms for gases and plasmas based on the Boltzmann equation and the Landau-Fokker-Planck equation*, Phys. Rev. E, 61 (2000), pp. 4576–4586.

[7] C. Buet and S. Dellacherie, *On the Chang and Cooper scheme applied to a linear Fokker-Planck equation*, Commun. Math. Sci., 8 (2010), pp. 1079–1090.

[8] J. A. Carrillo, M. Fornasier, G. Toscani, and F. Vecil, *Particle, kinetic, and hydrodynamic models of swarming*, in Mathematical Modeling of Collective Behavior in Socio-Economic and Life Sciences, G. Naldi, L. Pareschi, and G. Toscani, eds., Model. Simul. Sci. Eng. Technol., Birkhäuser, Boston, 2010, pp. 297–336.

[9] J. A. Carrillo, L. Pareschi, and M. Zanella, *Particle based gPC methods for mean-field models of swarming with uncertainty*, Commun. Comput. Phys., to appear; arXiv:1712.01677, preprint.

[10] J. S. Chang and G. Cooper, *A practical difference scheme for Fokker-Planck equations*, J. Comput. Phys., 6 (1970), pp. 1–16.

[11] S. Cordier, L. Pareschi, and G. Toscani, *On a kinetic model for a simple market economy*, J. Stat. Phys., 120 (2005), pp. 253–277.

[12] P. Degond, C. Appert-Rolland, J. Pettré, and G. Theraulaz, *Vision-based macroscopic pedestrian models*, Kinet. Relat. Models, 6 (2013), pp. 809–839.

[13] M. Delitala and A. Tosin, *Mathematical modeling of vehicular traffic: A discrete kinetic theory approach*, Math. Models Methods Appl. Sci., 17 (2007), pp. 901–932.

[14] L. Desvillettes, *On asymptotics of the Boltzmann equation when the collisions become grazing*, Transp. Theory Statist. Phys., 21 (1992), pp. 259–276.

[15] G. Dimarco, L. Pareschi, and M. Zanella, *Uncertainty quantification for kinetic models in socio-economic and life sciences*, in Uncertainty Quantification for Hyperbolic and Kinetic Equations, S. Jin and L. Pareschi, eds., SEMA SIMAI Springer Ser., Springer, New York, 2017.

[16] R. J. DiPerna and P. L. Lions, *On the Fokker-Planck-Boltzmann equation*, Comm. Math. Phys., 120 (1988), pp. 1–23.

[17] S. Fan, M. Herty, and B. Seibold, *Comparative model accuracy of a data-fitted generalized Aw-Rascle-Zhang model*, Netw. Heterog. Media, 9 (2014), pp. 239–268.

[18] L. Fermo and A. Tosin, *A fully-discrete-state kinetic theory approach to modeling vehicular traffic*, SIAM J. Appl. Math., 73 (2013), pp. 1533–1556.

[19] A. Festa, A. Tosin, and M.-T. Wolfram, *Kinetic description of collision avoidance in pedestrian crowds by sidestepping*, Kinet. Relat. Models, 11 (2018), pp. 491–520.

[20] G. Furioli, A. Pulvirenti, E. Terraneo, and G. Toscani, *The grazing collision limit of the inelastic Kac model around a Lévy-type equilibrium*, SIAM J. Math. Anal., 44 (2012), pp. 827–850.

[21] G. Furioli, A. Pulvirenti, E. Terraneo, and G. Toscani, *Fokker-Planck equations in the modeling of socio-economic phenomena*, Math. Models Methods Appl. Sci., 27 (2017), pp. 115–158.

[22] M. Herty, A. Fazekas, and G. Visconti, *A two-dimensional data-driven model for traffic flow on highways*, Netw. Heterog. Media, 13 (2018), pp. 217–240.

[23] M. Herty and L. Pareschi, *Fokker-Planck asymptotics for traffic flow models*, Kinet. Relat. Models, 3 (2010), pp. 165–179.

[24] S. P. Hoogendoorn, *Traffic Flow Theory and Simulation*, Lecture notes CT4821, Delft University of Technology, Delft, Netherlands, 2007.

[25] R. Illner, A. Klar, and T. Materne, *Vlasov-Fokker-Plank models for multilane traffic flow*, Commun. Math. Sci., 1 (2003), pp. 1–12.

[26] S. Jin and L. Pareschi, eds.. *Uncertainty Quantification for Hyperbolic and Kinetic Equations*, SEMA SIMAI Springer Ser. 14, Springer, New York, 2018.

[27] B. S. Kerner, *Synchronized flow as a new traffic phase and related problems for traffic flow modelling*, Math. Comput. Modelling, 35 (2002), pp. 481–508.

[28] A. Klar and R. Wegener, *Enskog-like kinetic models for vehicular traffic*, J. Stat. Phys., 87 (1997), pp. 91–114.
[29] A. Klar and R. Wegener, *Kinetic derivation of macroscopic anticipation models for vehicular traffic*, SIAM J. Appl. Math., 60 (2000), pp. 1749–1766.
[30] E. W. Larsen, C. D. Levermore, C. G. Pomraning, and J. G. Sanderson, *Discretization methods for one-dimensional Fokker-Planck operators*, J. Comput. Phys., 61 (1985), pp. 359–390.
[31] S. Maerivoet and B. De Moor, *Traffic Flow Theory*, Technical report, Katholieke Universiteit Leuven, 2005.
[32] S. Mishra, C. Schwab, and J. Šukys, *Multi-level Monte Carlo finite volume methods for uncertainty quantification in nonlinear systems of balance laws*, in Uncertainty Quantification in Computational Fluid Dynamics, Lect. Notes Comput. Sci. Eng. 92, Springer, New York, 2013, pp. 225–294.
[33] S. Moridpour, M. Sarvi, and G. Rose, *Lane changing models: A critical review*, Transp. Lett., 2 (2010), pp. 157–173.
[34] L. Pareschi, *Hybrid multiscale methods for hyperbolic and kinetic problems*, ESAIM Proc., 15 (2005), pp. 87–120.
[35] L. Pareschi and G. Russo, *An introduction to Monte Carlo method for the Boltzmann equation*, ESAIM Proc., 10 (2001), pp. 35–75.
[36] L. Pareschi and G. Toscani, *Interacting Multiagent Systems: Kinetic Equations and Monte Carlo Methods*, Oxford University Press, Oxford, 2013.
[37] L. Pareschi, G. Toscani, and C. Villani, *Spectral methods for the non cut-off Boltzmann equation and numerical grazing collision limit*, Numer. Math., 93 (2003), pp. 527–548.
[38] L. Pareschi, P. Vellucci, and M. Zanella, *Kinetic models of collective decision-making in the presence of equality bias*, Phys. A, 467 (2017), pp. 201–217.
[39] L. Pareschi and M. Zanella, *Structure preserving schemes for nonlinear Fokker-Planck equations and applications*, J. Sci. Comput., 74 (2018), pp. 1575–1600.
[40] S. L. Paveri-Fontana, *On Boltzmann-like treatments for traffic flow: A critical review of the basic model and an alternative proposal for dilute traffic analysis*, Transp. Res., 9 (1975), pp. 225–235.
[41] I. Prigogine, *A Boltzmann-like approach to the statistical theory of traffic flow*, in Theory of Traffic Flow, R. Herman, ed., Elsevier, Amsterdam, 1961, pp. 158–164.
[42] I. Prigogine and R. Herman, *Kinetic Theory of Vehicular Traffic*, American Elsevier, New York, 1971.
[43] G. Puppo, M. Semplice, A. Tosin, and G. Visconti, *Fundamental diagrams in traffic flow: The case of heterogeneous kinetic models*, Commun. Math. Sci., 14 (2016), pp. 643–669.
[44] G. Puppo, M. Semplice, A. Tosin, and G. Visconti, *Analysis of a multi-population kinetic model for traffic flow*, Commun. Math. Sci., 15 (2017), pp. 379–412.
[45] G. Puppo, M. Semplice, A. Tosin, and G. Visconti, *Kinetic models for traffic flow resulting in a reduced space of microscopic velocities*, Kinet. Relat. Models, 10 (2017), pp. 823–854.
[46] G. Toscani, *Kinetic models of opinion formation*, Commun. Math. Sci., 4 (2006), pp. 481–496.
[47] A. Tosin and M. Zanella, *Boltzmann-type models with uncertain binary interactions*, Commun. Math. Sci., to appear; arXiv:1709.02353), preprint.
[48] A. Tosin and M. Zanella, *Control strategies for road risk mitigation in kinetic traffic modelling*, IFAC-PapersOnLine, 51 (2018), pp. 67–72.
[49] C. Villani, *On a new class of weak solutions to the spatially homogeneous Boltzmann and Landau equations*, Arch. Ration. Mech. Anal., 143 (1998), pp. 273–307.
[50] C. Villani, *Conservative forms of Boltzmann's collision operator: Landau revisited*, ESAIM Math. Model. Numer. Anal., 33 (1999), pp. 209–227.
[51] G. Visconti, M. Herty, G. Puppo, and A. Tosin, *Multivalued fundamental diagrams of traffic flow in the kinetic Fokker-Planck limit*, Multiscale Model. Simul., 15 (2017), pp. 1267–1293.
[52] D. Xiu, *Numerical Methods for Stochastic Computations*, Princeton University Press, Princeton, NJ, 2010.
[53] D. Xiu and J. S. Hesthaven, *High-order collocation methods for differential equations with random inputs*, SIAM J. Sci. Comput., 27 (2005), pp. 1118–1139.
[54] D. Xiu and G. E. Karniadakis, *The Wiener–Askey polynomial chaos for stochastic differential equations*, SIAM J. Sci. Comput., 24 (2002), pp. 619–644.